2018

# Effects of Model Resolution and Ocean Mixing on Forced IceOcean Physical and Biogeochemical Simulations Using Global and Regional System Models

Jin, Meibing; Deal, Clara; Maslowski, Wieslaw; Matrai, Patricia; Roberts, Andrew; Osinski, Robert; Lee, Younjoo J.; Frants, Marina; Elliott, Scott; Jeffery, Nicole...

Wiley

http://hdl.handle.net/10945/57878

AGU PUBLICATIONS

JGR

Journal of Geophysical Research: Oceans

RESEARCH ARTICLE

10.1002/2017JC013365

**Key Points:**

- Model errors in mixed layer depth were reduced 36% by brine rejection parameterization, 20% by new ice processes, and 6% by higher resolution
- The modeled nitrate concentration biases in the Arctic Basin were caused by both mixed layer depth bias and coarse resolution
- Coarse resolution models may introduce excessive horizontal mixing of high nitrate from the Chukchi Sea into the Canada Basin

**Correspondence to:**
M. Jin,
mjin@alaska.edu

**Citation:**
Jin, M., Deal, C., Maslowski, W., Matrai, P., Roberts, A., Osinski, R., . . . Wang, S. (2018). Effects of model resolution and ocean mixing on forced ice-ocean physical and biogeochemical simulations using global and regional system models. *Journal of Geophysical Research: Oceans*, *123*, 358–377. https://doi.org/10.1002/2017JC013365

Received 15 AUG 2017
Accepted 22 DEC 2017
Accepted article online 28 DEC 2017
Published online 16 JAN 2018



# Effects of Model Resolution and Ocean Mixing on Forced Ice-Ocean Physical and Biogeochemical Simulations Using Global and Regional System Models

**Meibing Jin[1,2], Clara Deal[1], Wieslaw Maslowski[3], Patricia Matrai[4], Andrew Roberts[3], Robert Osinski[5], Younjoo J. Lee[3], Marina Frants[3], Scott Elliott[6], Nicole Jeffery[6], Elizabeth Hunke[7], and Shanlin Wang[6]**

[1]International Arctic Research Center, University of Alaska Fairbanks, Fairbanks, AK, USA, [2]Laboratory for Regional Oceanography and Numerical Modeling, Qingdao National Laboratory for Marine Science and Technology, Qingdao, China, [3]Department of Oceanography, Naval Postgraduate School, Monterey, CA, USA, [4]Bigelow Laboratory for Ocean Sciences, East Boothbay, ME, USA, [5]Institute of Oceanology, Polish Academy of Sciences, Sopot, Poland, [6]Computer, Computational, and Statistical Sciences Division, Los Alamos National Laboratory, Los Alamos, NM, USA, [7]Theoretical Division, Los Alamos National Lab, Los Alamos, NM, USA

**Abstract** The current coarse-resolution global Community Earth System Model (CESM) can reproduce major and large-scale patterns but is still missing some key biogeochemical features in the Arctic Ocean, e.g., low surface nutrients in the Canada Basin. We incorporated the CESM Version 1 ocean biogeochemical code into the Regional Arctic System Model (RASM) and coupled it with a sea-ice algal module to investigate model limitations. Four ice-ocean hindcast cases are compared with various observations: two in a global 1° (40∼60 km in the Arctic) grid: G1deg and G1deg-OLD with/without new sea-ice processes incorporated; two on RASM's 1/12° (∼9 km) grid R9km and R9km-NB with/without a subgrid scale brine rejection parameterization which improves ocean vertical mixing under sea ice. Higher-resolution and new sea-ice processes contributed to lower model errors in sea-ice extent, ice thickness, and ice algae. In the Bering Sea shelf, only higher resolution contributed to lower model errors in salinity, nitrate ($NO_3$), and chlorophyll-a (Chl-a). In the Arctic Basin, model errors in mixed layer depth (MLD) were reduced 36% by brine rejection parameterization, 20% by new sea-ice processes, and 6% by higher resolution. The $NO_3$ concentration biases were caused by both MLD bias and coarse resolution, because of excessive horizontal mixing of high $NO_3$ from the Chukchi Sea into the Canada Basin in coarse resolution models. R9km showed improvements over G1deg on $NO_3$, but not on Chl-a, likely due to light limitation under snow and ice cover in the Arctic Basin.

## 1. Introduction

The Arctic Ocean is warming more rapidly than other regions on the Earth and there is already evidence of corresponding marine ecosystem response, such as the northward shift of subarctic and arctic marine communities (Grebmeier et al., 2006) in the Pacific Arctic, an intensive under-ice phytoplankton bloom (Arrigo et al., 2012) in the marginal ice zone, a shift in phytoplankton community composition toward smaller cells (Li et al., 2009) and an increased vertical export of algal biomass (Boetius et al., 2013) in the Arctic Basin. Increasing temperature, open water area, and duration have triggered increased primary production (PP) in the open waters of the Arctic Ocean, as observed by remote sensing (Arrigo et al., 2011; Pabi et al., 2008). These large-scale trends can be simulated by climate models even at coarse resolution, e.g., a 1° global grid with Los Alamos National Laboratory's sea-ice model (CICE) and Parallel Ocean Program (POP), as described in Jin et al. (2012a, 2016). Increasing computer power has enabled the development of high-resolution climate models that are assumed to better simulate ocean mixing and circulation near sharp bathymetric features, and transport (heat, salt, and other tracers) through narrow channels (e.g., the Bering and Fram Straits). However, the benefits to both physical and biological models have yet to be fully assessed, e.g., what are the temporal and spatial distributions (beyond bathymetric features and narrow channels) of the benefits and are they different for different tracers?

Using a varying resolution regional model (minimum 4 km near the Alaska's coast), Zhang et al. (2015) found that under-ice blooms in the Chukchi Sea increased in recent decades due to both increasing light

availability related to reducing sea-ice cover, and nutrient supply from the shelf break due to an intensifying circulation, which is weaker in coarse resolution models. Arctic ecosystem model intercomparison studies (Jin et al., 2016; Lee et al., 2015, 2016) also show that models with horizontal resolutions from 1 to 0.25°, and even higher for regional models, could simulate the mean states of the seasonal cycle of PP but with less variability compared to in situ observations. But even with a general agreement of annual PP levels among models and observations, Popova et al. (2012) found that different models with biogeochemistry disagreed on the sources and strength of limiting factors (light versus nutrients). The scatter of the modeled present-day Arctic Ocean nutrients in climate models has led to large uncertainties in the future projection of Arctic PP (Vancoppenolle et al., 2013), as the phytoplankton limiting factors switch from light to nutrients due to projected declining sea-ice cover in the future. Model biases in surface seawater nitrate concentration ($NO_3$) were likely due to an unrealistic representation of ocean physics, such as circulation, mixing, sea-ice processes, and biogeochemical parameterizations (Popova et al., 2012; Vancoppenolle et al., 2013).

Subsurface chlorophyll-a maxima (SCM) have been underestimated in satellite-based estimations of Arctic Ocean PP (Arrigo & van Dijken, 2011). Failure to simulate SCM could be due to either too much nitrate and hence no surface limitation or too little nitrate with limited surface growth (Steiner et al., 2016). An extensive comparison of 21 regional and global ecosystem models against observations in the Arctic (1959–2011) by Lee et al. (2016) evaluated modeled net primary productivity (NPP) and environmental variables such as $NO_3$, mixed layer depth (MLD), euphotic layer depth, and sea-ice concentration. They found that models tend to perform relatively well at simulating NPP in the Beaufort Sea and central Arctic Basin, but less well in the Greenland and Chukchi Seas, despite the higher model skill in MLD and sea-ice concentration in this region. Since models in the above intercomparison differed not only in the grids used but also in their representation of physical and biological processes and the choice of parameters, it is hard to pinpoint underlying mechanisms or parameterizations among different models. It is therefore critical to examine the different effects of spatial resolution, sea-ice model processes, and ocean vertical mixing parameterization on the simulation of the Arctic biogeochemical cycling, by comparing simulations using the same code but different resolutions and choices of parameters.

The advancement of supercomputer power enables climate models to test increased spatial resolution from coarse, noneddy resolving toward eddy permitting or even eddy resolving grids (<10 km resolution in the Arctic Basin). Still, the computational cost usually favors higher resolution only in smaller domains. It is important to investigate where spatial resolution is critically needed and understand the compatibility of model parameters with increased resolution. There are many small-scale physical processes, such as mesoscale eddies, mixed layer dynamics, coastal and boundary currents, upper ocean stratification, and marginal ice zone expansion that influence nutrient transport, light availability and ocean stratification, which are critical to marine PP and carbon cycling in the Arctic Ocean. Such physical processes, and feedbacks among

**Table 1**
*Differences Between the Model Case Configurations*

| | R9km | R9km-NB | G1deg | G1deg-OLD |
|---|---|---|---|---|
| Domain and resolution | Regional Pan Arctic. Horizontally ~9 km, 45 vertical layers: 5 m in top 20 m, increasing to 250 m at the bottom. | | Global domain. Horizontally 1° (approximately 40~50 km in the Arctic), 60 vertical layers: 10 m in top 150 m increasing to 250 m at the bottom. | |
| Subgrid brine rejection parameterization (Jin et al., 2012b) | Yes | No | Yes | Yes |
| Ocean-ice coupling time | 20 min | 20 min | 1 h | 1 day |
| Elastic subcycling time step (Hunke, 2001) | 2 s | 2 s | 10 s | 10 s |
| Thermodynamics | Prognostic salinity (Turner & Hunke, 2015) | | | Diagnostic salinity (Bitz & Lipscomb, 1999) |
| Melt ponds | Level Ice (Hunke et al., 2013) | | | Virtual (Holland et al., 2012) |
| Delta-Eddington snow grain adjustment (Briegleb & Light, 2007 | $r_{snow} = 0.50$ | | | $r_{snow} = 1.75$ |
| Rheology | EAP (Wilchinsky & Feltham, 2004) | | | EVP (Hunke & Dukowicz, 1997) |
| Frictional loss (Lipscomb et al., 2007) | $C_f = 21.3$ | | | $C_f = 17.0$ |

*Note*. All other model settings not listed, such as the model code and atmospheric forcing, are the same for all cases.

them, might be intimately involved in the recent dramatic changes observed in the Arctic, yet understanding of their representation in state-of-the-art global climate and earth system models is still limited.

The main motivation of this study is to examine the effects of some key physical model processes (e.g., sea-ice model parameters which strongly affect ice extent and thickness, ocean horizontal and vertical mixing, etc.) on biogeochemical simulations in the Arctic Ocean. In order to identify the causes of model errors in the physical and biogeochemical fields, we compared outputs from four ice-ocean model runs, all of which use the same CICE and POP updated codes including ocean lower-trophic-level ecosystem and biogeochemical cycling (BGC, Jin et al., 2012a, 2016; Moore et al., 2013) modules, and forced by the same atmospheric data. This study focused on model spatial resolution and model processes selected from newly available POP and CICE model updates. These factors can significantly affect ocean mixing which has been shown to influence the modeled Arctic nutrient bias described in Popova et al. (2012). The model processes are organized into two categories: (1) the brine rejection parameterization in POP and (2) a group of parameters in CICE and the POP's coupling time with CICE and atmospheric forcing data (see Table 1 for details).

## 2. Physical and Biogeochemical Model Configurations

### 2.1. Physical Model

In this study, we use the ice-ocean model components of RASM in its native regional domain grid (e.g., Cassano et al., 2017; Hamman et al., 2017; Roberts et al., 2015) and in a global domain grid from CESM. The RASM domain (Figure 1) covers the entire Northern Hemisphere marine cryosphere, major oceanic inflow and outflow pathways, with optimal extension into the North Pacific and Atlantic oceans to account for the origin and passage of cyclones over marginal ice zones and into the Arctic. The RASM ocean and sea-ice models are POP version 2 and CICE version 5.1.2, respectively. With a focus on examining ice-ocean biophysical model efficiencies using validation with observations, we use reanalysis data forced ice-ocean model configurations instead of fully coupled ocean-ice-atmosphere-land-BGC simulations; therefore we only describe the POP and CICE models in this paper.

In contrast to POP and CICE in CESM version 1.1, RASM has incorporated the following new model innovations. In POP, subgrid scale brine rejection parameterization (Jin et al., 2012b) is implemented to improve ocean vertical mixing under sea-ice cover. In CICE, the following adjustments were made: (1) "mushy-layer" thermodynamics (Turner & Hunke, 2015); (2) new thermodynamic coupling to the ocean, whereby the basal freezing temperature is identical to the temperature of the liquid phase within sea ice, rather than set at a fixed temperature of −1.8°C in CESM Version 1; (3) explicit level ice ponds instead of virtual melt ponds in CESM Version 1, and (4) Wilchinsky and Feltham (2004) Elastic Anistropic Plastic (EAP) sea-ice rheology instead of the Elastic Viscous Plastic (EVP) mechanics of Hunke and Dukowicz (1997), with the frictional parameter ($C_f$) adjusted to increase mechanical dissipative loss, following Tsamados et al. (2013). The RASM ice-ocean components also differ in their coupling methods. While both CESM Version 1 and RASM utilize the coupler of Craig et al. (2012), the ice-ocean coupling step is either daily or hourly in CESM, but 20 min in the RASM 9 km grid to resolve coupled ice-ocean inertial oscillations (Roberts et al., 2015). Atmospheric forcing data are linearly interpolated to each time step in the model.

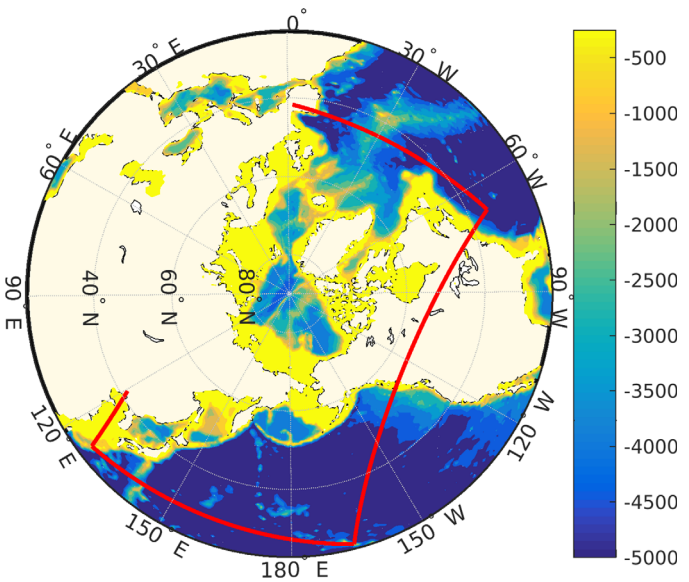


**Figure 1.** The RASM ocean and sea-ice model domain is shown by the red line bounded box and the colors denote the ocean bathymetry.

In order to fully examine the effects of model spatial resolution and physical processes in ocean and sea ice on the BGC model performance, we configured four comparison cases with differences shown in Table 1:

(1) R9km: RASM 1/12° (~9 km) ice-ocean regional grid (Figure 1); (2) G1deg: nominally 1° global grid adopted from CESM used in Hurrell et al. (2013) with a varying resolution of 40–111 km grid from the polar to tropical regions; (3) R9km-NB: the same as R9km except turning off the subgrid scale brine rejection parameterization (Jin et al., 2012b) that improves ocean mixing under sea-ice cover; and (4)

G1deg-OLD: the same as G1deg except using the old parameter set for CICE version 4 and a daily coupling time between POP and coupler. Note that R9km and G1deg are the control runs for the 9 km regional grid and 1° global grid, respectively, while R9km-NB and G1deg-OLD are comparison cases with old physics of the POP and CICE, similar to those used in previous Arctic ecosystem model studies (Jin et al., 2012a; Popova et al., 2012). Cases 1 and 2 are used to examine the model improvement due to increased resolution. Cases 3 and 4 are used to examine the recent development of sea ice and ocean models and their effects on ocean vertical mixing (represented by MLD) and biogeochemical simulations in the Arctic Ocean.

### 2.2. Biogeochemical Model

The biogeochemical cycling module consists of linked pelagic and sea-ice algal components (Jin et al., 2012a, 2016). The ice algal component represents assemblages in a 3 cm layer at the bottom of each sea-ice thickness category, coupled to the pelagic model through nutrient and biotic fluxes. This submodel was first developed based on fast-ice core data collected offshore Barrow, Alaska (Jin et al., 2006). It has been tested and validated through coupling with a 1D column pelagic ecosystem model in the southeastern Bering Sea (Jin et al., 2007) and the Chukchi and Beaufort Seas (Lee et al., 2010), global CICE with a simple slab ocean model (Deal et al., 2011), and the aforementioned global coupled POP-CICE and 3D pelagic ecosystem configuration (Jin et al., 2012a). The ice algal model includes six components: ice algae, three nutrients ($NO_3$, ammonium ($NH_4$) and silicate (Si)), and two biogenic sulfur compounds (dimethylsulfide (DMS), and dimethylsulfoniopropionoate (DMSP); see Elliott et al., 2012). The sea-ice physical model computes the thermodynamic and dynamic properties of the ice in each grid cell using a multicategory ice thickness distribution method (Hunke et al., 2015). The biological model is solved with the physical input of ice thickness growth rate, temperature, salinity, and light intensity in the bottom ice layer. The biological variable in a grid cell is the sum over each ice thickness category (there are five categories representing thinnest to thickest ice in each grid cell). Horizontal advection of biological constituents is calculated for each ice category using the same numerical scheme as tracers in the sea-ice physical model. Transport across the water-ice interface is represented as the lower boundary condition for the sea-ice BGC model.

The pelagic BGC component is a medium-complexity Nutrients-Phytoplankton-Zooplankton-Detritus (NPZD) model (Moore et al., 2002, 2004, 2013), with multiple phytoplankton functional groups including diatoms, small phytoplankton (flagellates), and diazotrophs, to accommodate diverse ecological regimes around the globe; bacterial activity is implicit in the nutrient and organic carbon remineralization rates. The model includes 24 state variables: $NO_3$, $NH_4$, iron (Fe), Si, phosphate ($PO_4$), three types of phytoplankton (explicit carbon, Fe, and chlorophyll-a pools for each phytoplankton functional group, an explicit Si pool for diatoms and an implicit $CaCO_3$ pool for small phytoplankton, totaling 11 state variables), a herbivorous zooplankton pool, dissolved organic nitrogen, carbon, iron, and phosphate (DON, DOC, DOFe, DOP), oxygen ($O_2$), dissolved inorganic carbon (DIC), and alkalinity.

### 2.3. Model Numerical Settings

All model cases use the same sea-ice thickness configuration of five thickness categories, with gradations as described in Roberts et al. (2015). The atmospheric forcing and river runoff are prescribed from the reanalysis Coordinated Ocean-ice Reference Experiment Forcing Version 2.0 (CORE-II) data from 1948 to 2009 (Large & Yeager, 2009). Model temperature and salinity along the RASM 9 km lateral boundaries are restored to the monthly Polar science center Hydrographic Climatology (PHC 3.0, Steele et al., 2001) data with a time scale of 30 days.

Initial conditions for ocean T and S are from PHC, and nutrient variables ($NO_3$, Si) are from the gridded World Ocean Atlas (WOA2013) on the National Oceanic and Atmospheric Administration (NOAA) web site https://www.nodc.noaa.gov/OC5/woa13/woa13data.html. The initial conditions for other ecosystem components are from the recent version of CESM global 1° grid initial conditions (Moore et al., 2013). All model runs start from 1965 with no motion in the ocean and no sea ice to 1975, then restart with the sea-ice field of 1975 but no motion in ocean and initial T and S. This approach was used in model simulations by Steiner et al. (2016) to reduce the effects of initial ice formation on the ocean T and S field. Only the model results from 1980 onward were used for model-data comparison as observational data used in this study start from 1980, though most data were collected after 2000.

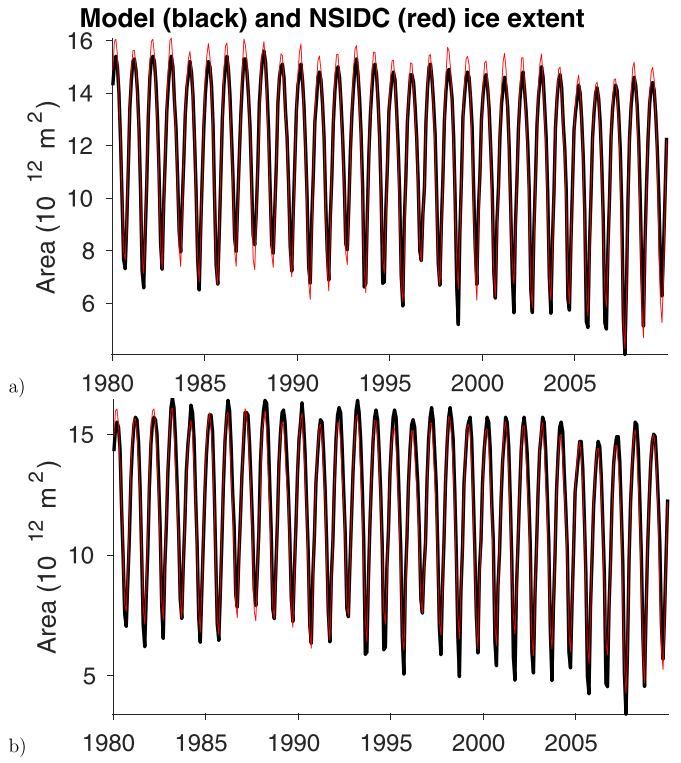


**Figure 2.** Model comparison of monthly mean northern hemisphere sea-ice extent with NSIDC data: (a) R9km and (b) G1deg.

## 3. Model Results

The RASM sea ice and ocean physical model results have been validated in various previous studies (Cassano et al., 2017; DuVivier et al., 2016; Hamman et al., 2017; Roberts et al., 2015). However, since the marine ecosystem model results are significantly affected by the simulated sea ice and ocean physical environments, we also include physical model validations and comparisons.

### 3.1. Sea Ice and Ice Algae

Both R9km and G1deg simulated well the seasonal and interannual changes of the monthly mean northern hemisphere sea-ice extent as compared with the remote sensing data (Figure 2) from the National Snow and Ice Data Center (NSIDC). The root mean square errors (RMSE; the smaller the RMSE, the better the model performs) over the 30 year (1980–2009) period are shown in Table 2. The ice extents are almost the same for the R9km and R9km-NB cases, because the brine rejection parameterization improves mostly on ocean vertical mixing under pack ice, but less on the marginal ice zone and sea-ice extent. The ice extent RMSE of the R9km and R9km-NB cases are 25% lower than that of G1deg, and the RMSE of G1deg is 10% lower than that of G1deg-OLD, indicating that both increasing spatial resolution and enhancing sea-ice model processes play important roles in improving sea-ice extent simulation. The RMSEs of monthly mean ice extent for R9km are generally lower than those for G1deg (Table 2) except for January, February, March, and October. The superior performance of R9km in spring to fall months provides a more realistic basis for biogeochemical simulations since the major bloom period in the Arctic Ocean is from May to September (Jin et al., 2016).

Sea-ice thickness was derived from upward looking sonar (ULS) data at three multiyear mooring stations A, B, and C (locations in Figure 3a) in the Canada Basin (Krishfield et al., 2014). The simulated sea-ice thickness for R9km and G1deg (Figures 3b and 3c) agrees in timing and magnitude with the observed seasonal cycles most of the time. The RMSE is 45 cm for R9km, lower than the other cases which are 52, 51, and 99 cm for R9km-NB, G1deg, and G1deg-OLD, respectively. The sea-ice model process improvements (G1deg versus G1deg-OLD) led to a significant RMSE reduction in simulated ice thickness. Individually, the brine rejection parameterization and increasing resolution can reduce the ice thickness RMSE by about 5% for the three stations in the Canada Basin. The modeled 5 year (2005–2009) average ice thickness in the pan-Arctic from January to March (Figure 4) are the thickest in G1deg-OLD. Note that the relative ice thickness between model cases in other seasons (spring, summer, and fall) are similar to that in winter and hence not shown here. The ice thickness in R9km is similar to R9km-NB overall and only slightly thicker in the East Siberian Sea. The ice thickness in G1deg is thicker than R9km in the Beaufort Gyre region, but thinner in the East Siberian Sea and eastern Arctic Ocean.

Sea-ice thickness, snow depth, sea surface $NO_3$ concentration, and ice algal biomass were measured on the offshore fast ice west of Utqiagvik (formerly Barrow) (station D in Figure 3a) in 2002 and 2003 (Jin et al.,

**Table 2**
*Model RMSE of Monthly Northern Hemisphere Ice Extent ($10^{11} m^2$) and RMSE of All Data in the Last Column*

| Month | 1 | 2 | 3 | 4 | 5 | 6 | 7 | 8 | 9 | 10 | 11 | 12 | All data |
|---|---|---|---|---|---|---|---|---|---|---|---|---|---|
| R9km | 4.9 | 6.7 | 5.3 | **2.9** | **3.3** | **4.8** | 7.8 | **6.5** | **5.6** | 6.2 | **2.1** | **2.7** | **5.2** |
| R9km-NB | 4.9 | 6.7 | 5.3 | 2.9 | 3.3 | 4.9 | 7.6 | 7.0 | 5.9 | 6.2 | 2.2 | 2.7 | 5.3 |
| G1deg | 2.7 | 2.9 | 4.2 | 8.6 | 11.0 | 7.2 | 9.6 | 7.9 | 8.0 | 4.3 | 2.6 | 3.2 | 6.7 |
| G1deg-OLD | 2.8 | 3.8 | 6.9 | 11.4 | 13.3 | 7.4 | 10.6 | 6.9 | 5.9 | 5.2 | 2.5 | 3.3 | 7.5 |

*Note*. The bold numbers denote less RMSE for R9km.

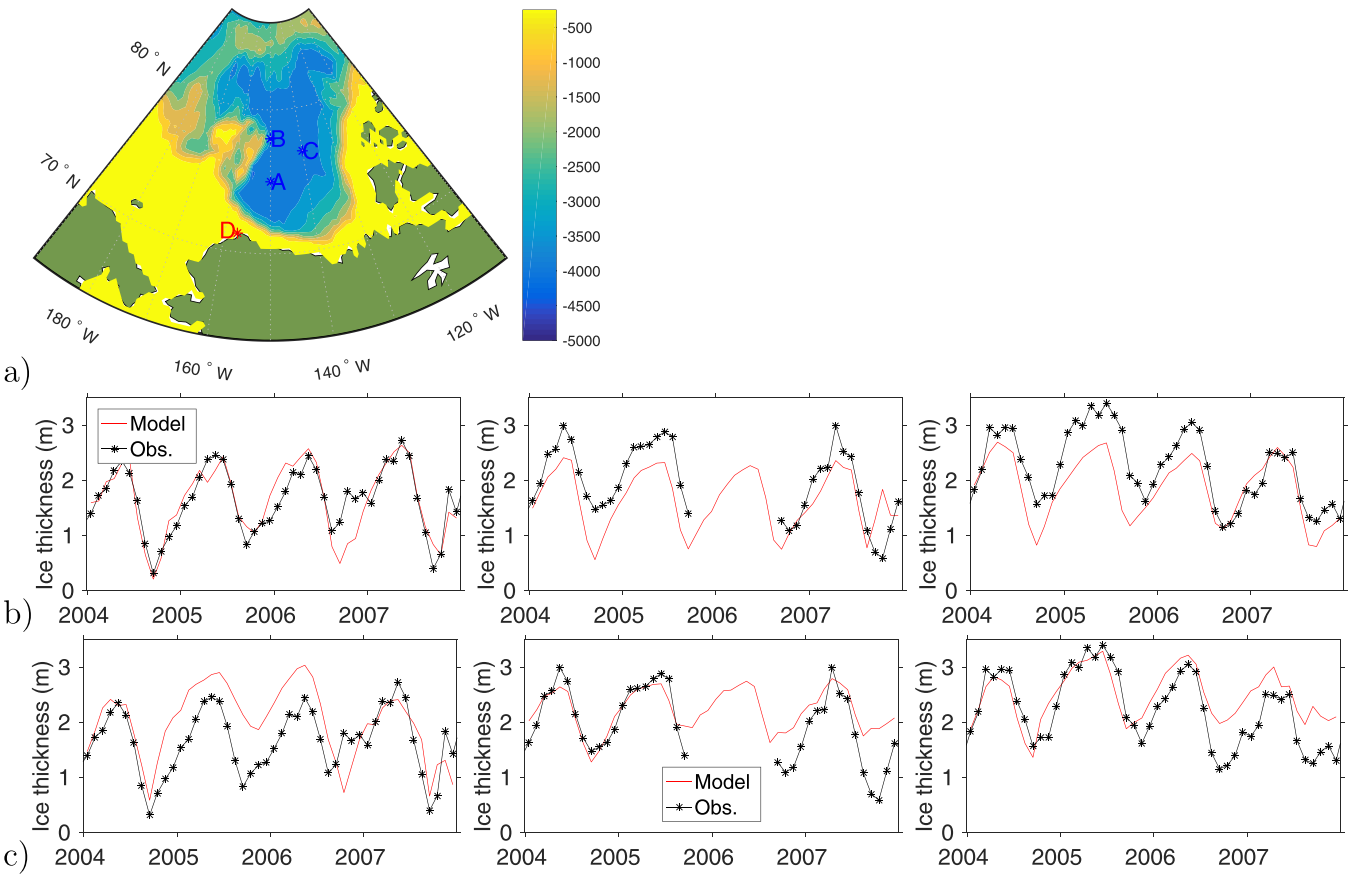


**Figure 3.** (a) Sea-ice thickness was measured at stations A, B, and C in the Beaufort Sea. Model comparisons with observed monthly mean sea-ice thickness at stations A, B, C from left to right, respectively: (b) R9km (RMSE = 45 cm) and (c) G1deg (RMSE = 51 cm). The red "D" denotes the location of the fast ice station used in Figure 5.

2006). Note that the existing versions of the sea-ice model, CICE, are not capable of simulating landfast ice, due to the lack of a mechanism for a small (subgrid size) ice keel to ground on the shallow ocean bottom and a subsequent trigger mechanism for the grounded ice to break free. Another challenge is that landfast ice along the Alaska coast is often too narrow, even for a higher-resolution case to resolve. Further development of the ice model is needed to improve this aspect of sea-ice simulations. The modeled sea-ice thickness for the nearest point near this location (Figure 5a) shows much larger temporal variations than observed in winter, as the ice was mobile in the model. The R9km-NB displays negligible differences from R9km for all variables in Figure 5 and therefore is not shown here. The sea-ice thickness variations are similar between R9km and G1deg, and relatively larger than in G1deg-OLD, in winter, because of the different ice processes and parameters in G1deg-OLD. This suggests that sea-ice processes play a more important role than spatial resolution in the temporal variation of simulated ice thickness. The modeled snow depth (Figure 5b) compares reasonably well with observations for R9km but less so for G1deg and G1deg-OLD. The modeled sea surface $NO_3$ concentration (Figure 5c) shows good agreement with the few existing observations during ice melt, with a sharp decline in concentration at the end of the ice algal bloom in late May for all cases. The $NO_3$ concentration before the decline was overestimated in R9km and underestimated in G1deg and G1deg-OLD. The lower nutrients and thicker snow depth in G1deg and G1deg-OLD led to lower magnitudes of ice algal biomass than in R9km and observations (Figure 5d).

There were two spring (March–May) cruises in the Bering Sea (ice core stations in Figure 6a) during the Bering Sea Ecosystem Studies (BEST) program (Szymanski & Gradinger, 2016). The ice algal measurements were made at 1 or 2 cm vertical intervals in the bottom 5–10 cm and at 10 cm intervals above 10 cm. The ice algal chlorophyll-a concentration (Chl-a) reached above 1,000 mg/m$^3$ in the bottom 3 cm but dropped rapidly to less than 10% above 10 cm for most of the ice cores. The model output for the skeletal layer,

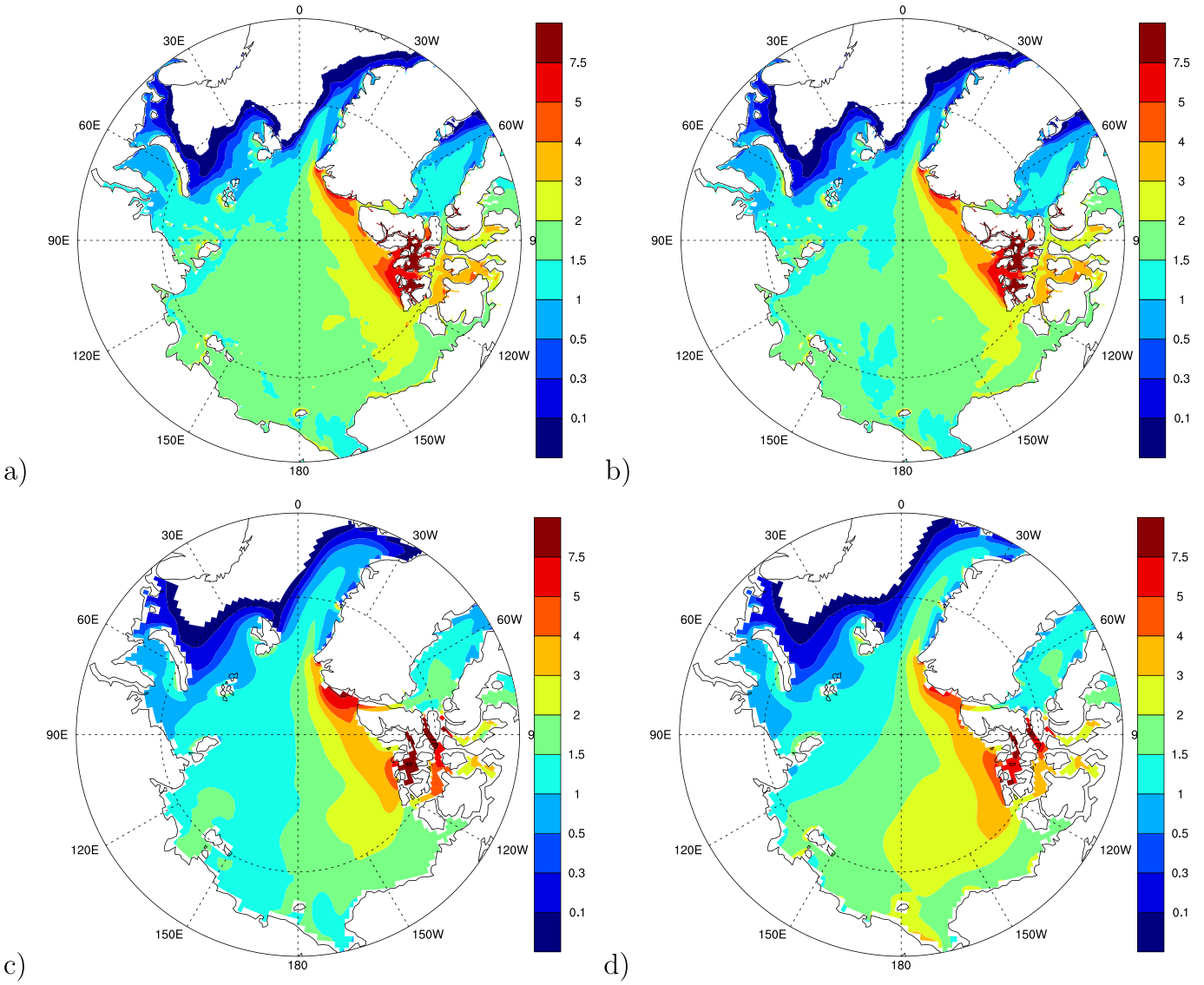


**Figure 4.** (a) January–March averaged 5 year mean (2005–2009) sea-ice thickness (m) from (a) R9km; (b) R9km-NB; (c) G1deg; and (d) G1deg-OLD.

representing the bottom 3 cm ice algal Chl-a concentrations, is compared to average measurements in the bottom 3 cm in 2008 and 2009 (Figure 6b). The R9km-NB case had negligible differences with R9km and is not shown in the figure. In 2008, all model cases show similar results that are comparable to the variations of the observations, but with higher maxima and lower minima than the observations. For 2009, R9km model results match the observations more closely than G1deg and G1deg-OLD in March to early April, but similarly afterward. All model cases capture the spatial variations between stations, especially for the R9km in 2009.

### 3.2. Ocean Environmental Conditions and Phytoplankton Bloom

The RMSE of modeled sea surface variables (temperature (SST), salinity, and $NO_3$ and Chl-a concentrations) (Table 3) were calculated against the BEST cruise data in March to May of 2008 and 2009 (stations shown in Figure 7a). The RMSE (Table 3) are generally similar for the same resolution model cases. The RMSE for higher-resolution model cases are lower for salinity, $NO_3$, and Chl-a, but higher for SST. Since salinity is the main control on ocean stratification in winter, RMSE of $NO_3$ and Chl-a for R9km are also smaller. The Taylor diagram (Taylor 2001) with normalized standard deviation, root-mean-square difference

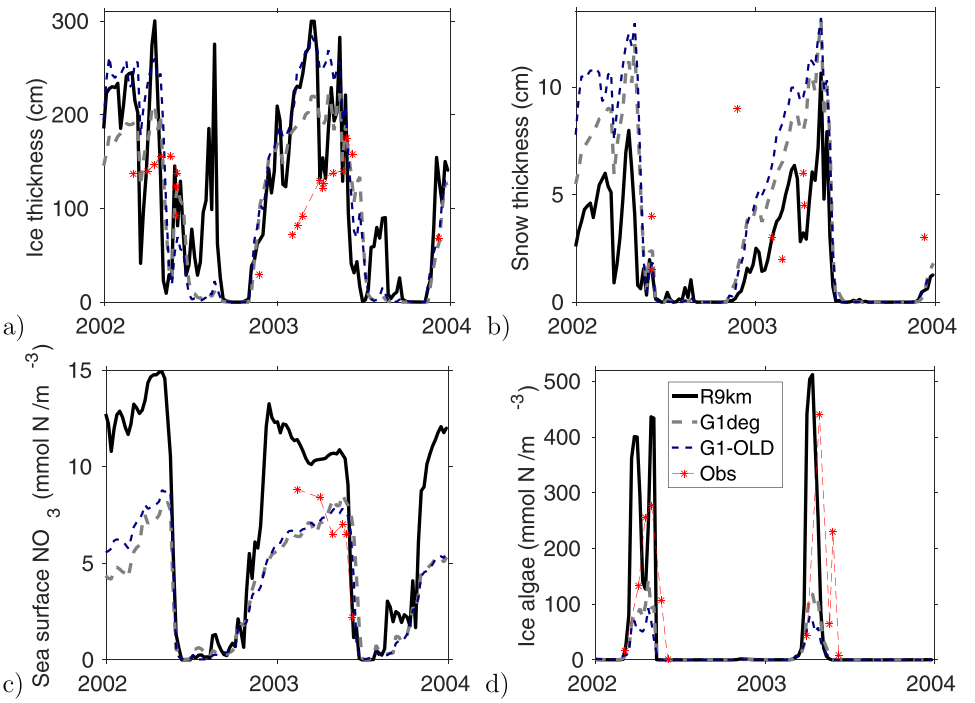


**Figure 5.** Model comparison with observations at the station to the west of Barrow (red "D*" in Figure 3a): (a) ice thickness; (b) snow depth; (c) sea surface $NO_3$; and (d) ice algal biomass in the skeletal layer.

(RMSD=$\sqrt{\frac{1}{N}\sum\left[(C-\bar{C})-(C_r-\bar{C_r})\right]^2}$, which is slightly different from RMSE=$\sqrt{\frac{1}{N}\sum(C-C_r)^2}$; here $C$ and $C_r$ denote the modeled and observational variables, respectively) and correlation coefficient (Figure 7b) shows that R9km had better model-data correlations for all four variables and smaller RMSD except for

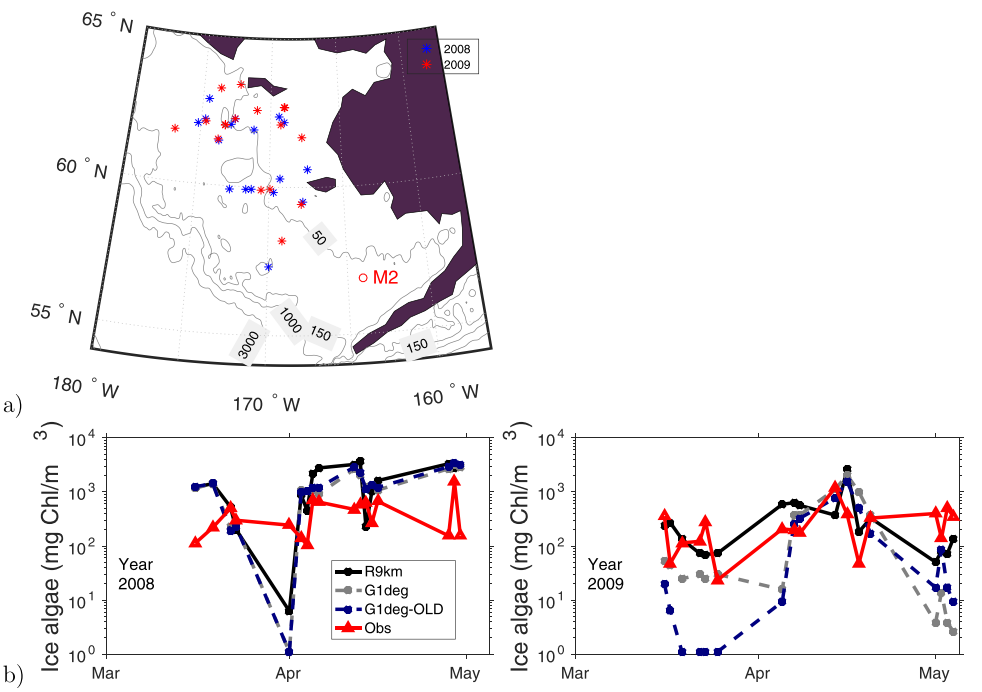


**Figure 6.** (a) Map of ice core measurement stations ("*") and M2 mooring station ("o") in the Bering Sea. (b) Modeled ice algal biomass comparison with ship observations in 2008 and 2009.

**Table 3**
*Model RMSE for Sea Surface Temperature, Salinity, $NO_3$ and Chl-a at the BEST Stations in the Bering Sea from March to May of 2008 and 2009*

| | Temperature (°C) | Salinity (psu) | $NO_3$ (mmol/m$^3$) | Chl-a (mg/m$^3$) |
|---|---|---|---|---|
| R9km | 0.65 | 0.29 | 7.73 | 0.89 |
| R9km-NB | 0.89 | 0.32 | 7.78 | 0.89 |
| G1deg | 0.48 | 0.70 | 8.52 | 1.04 |
| G1deg-OLD | 0.47 | 0.70 | 8.29 | 1.00 |

temperature, similar to the RMSE results. The standard deviations (representing variability) for R9km are closer to observations for salinity and $NO_3$, but larger for SST and smaller for Chl-a when compared to G1deg. The large errors in modeled $NO_3$ are mainly because the modeled phytoplankton bloom started later than observed at some stations, where observed $NO_3$ were drawn down to low levels while modeled $NO_3$ were still at prebloom highs (around 10–15 mmol/m$^3$). A 10% reduction in the $NO_3$ RMSE for the R9km case over the coarse resolution model case G1deg reveals that the simulation of $NO_3$ concentrations can be improved, although the absolute errors are still large for the current models. The improvements may come from better simulated ocean mixing, e.g., direct mixing of nutrients and biological consumption of nutrients under improved bloom timing which depends on stratification (or ocean mixing) conditions.

The seasonal cycles of phytoplankton biomass in the Bering Sea are characterized by a strong but brief period of pulse-like blooms in the spring time. This is illustrated in the comparisons (Figure 8) of model results of R9km and G1deg with remotely sensed sea surface Chl-a from daily mean Sea-viewing Wide Field-of-view Sensor (SeaWiFS) data (from NASA web site, https://oceancolor.gsfc.nasa.gov/) and relative fluorescence data from the M2 mooring at 12 m depth (Stabeno et al., 2001) in 2003 and 2004. The Chl-a results are only slightly different between R9km and G1deg, and almost the same between the same spatial resolution cases (not shown). The fluorescence data (volt units) were scaled to have the same maximum as the model Chl-a in Figure 8, to compare the relative changes in magnitude. The simulated bloom timing and magnitude in both R9km and G1deg showed a comparable range of values to the remotely sensed Chl-a concentration in the top optical depth and in the subsurface 12 m layer. Although R9km showed improvements in modeled salinity, nutrients, and Chl-a over G1deg in Figure 7, the phytoplankton bloom differences between the high and coarse resolution model cases (Figure 8) were actually small, suggesting that model resolution is not critical on the broad Bering Sea shelf, possibly due to the gentle bathymetric slope. The modeled bloom period at the sea surface is close to that of remotely sensed Chl-a, but the bloom duration at 12 m is narrower than that from the fluorescence measurements.

### 3.3. Mixed Layer Depth, Nutrients, and Primary Production

An earlier arctic biogeochemical model intercomparison (Popova et al., 2012) identified model errors in surface nitrate concentration in the Arctic Basin as a major deficiency that may be caused by unrealistic representation of ocean physics, in particular vertical mixing due to commonly overestimated MLD. The four model cases are compared with 29 year-long ice-tethered profilers (ITP) in the Arctic Basin (Toole et al., 2010; a list of deployment time periods in Table 4 and tracks in Figure 9a) to investigate the effects of model

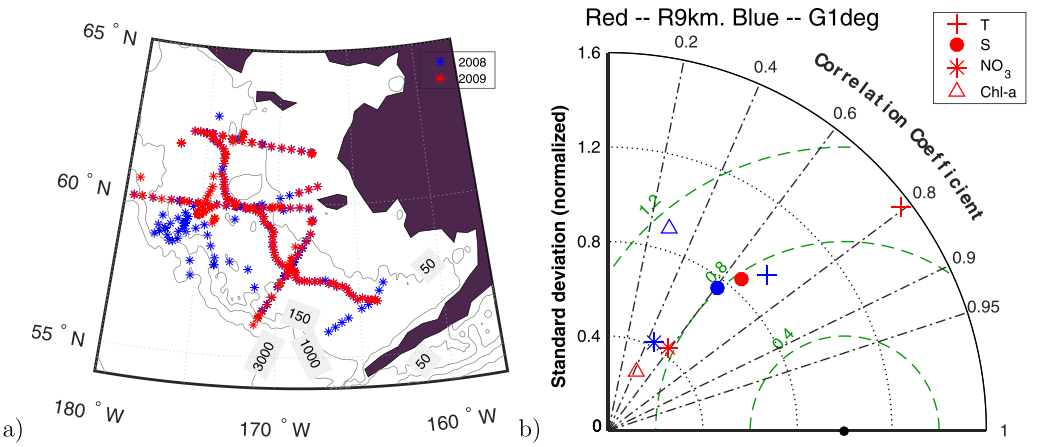


**Figure 7.** (a) Map of in situ ocean measurement stations ("*") in the Bering Sea. (b) Taylor diagram of the normalized standard deviation (meridional direction, 1 denotes the closest to observation) and correlation coefficient (zonal direction, 1 denotes the best correlation between model and observation) and bias (the contour lines, the smaller the better) of the ocean surface temperature, salinity, $NO_3$ and Chl-a.

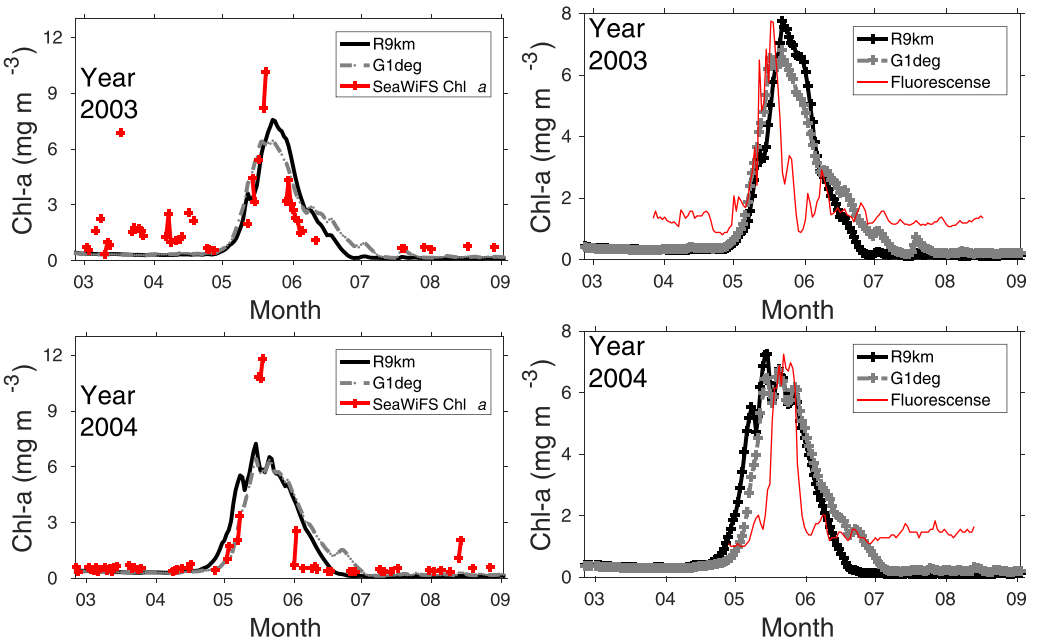


**Figure 8.** (left column) Model comparison with SeaWiFS sea surface Chl-a and (right column) 12 m depth fluorescence data at mooring station M2 in the Bering Sea (location shown in Figure 6a).

resolution, sea-ice processes, and brine rejection parameterization on the simulated MLD. The MLD was calculated from ITP temperature and salinity profiles, using the same method as in POP (Large et al., 1997). Note that ITPs can reach only 7–8 m below the sea surface to avoid hitting sea ice, so the surface density needed for reference in those calculations might be overestimated, resulting in deeper MLD estimates than from in situ data (Peralta-Ferriz & Woodgate, 2005). The model RMSE of MLD (at the same date and location as the ITP data) against all 29 ITP data sets are 10.4, 16.3, 11.1, and 14.0 m for R9km, R9km-NB, G1deg, and G1deg-OLD, respectively. R9km and R9km-NB showed the lowest and highest MLD errors, and the brine rejection parameterization resulted in a 36% reduction of the simulated MLD RMSE. The sea-ice processes improvement from G1deg-OLD to G1deg (Table 1) led to a 20% reduction of MLD RMSE, and the indirect influences of changing sea ice thermodynamics/dynamics on ocean mixing deserve further study in the

**Table 4**
*List of ITP Data: The ITPs are Numbered in the Order of Deployment Time in the Arctic Ocean*

| ITP number | Starting time | Ending time | ITP number | Starting time | Ending time |
|---|---|---|---|---|---|
| 1 | 2005.08.16 | 2007.01.06 | 19 | 2008.04.08 | 2008.11.21 |
| 3 | 2005.08.24 | 2006.09.08 | 21 | 2008.08.04 | 2009.09.23 |
| 4 | 2006.09.03 | 2007.08.17 | 23 | 2008.08.05 | 2010.07.06 |
| 5 | 2006.09.08 | 2007.09.06 | 24 | 2008.10.03 | 2009.09.25 |
| 6 | 2006.09.05 | 2008.06.23 | 25 | 2008.09.22 | 2009.07.07 |
| 7 | 2007.04.28 | 2007.10.24 | 26 | 2008.09.11 | 2009.03.11 |
| 8 | 2007.08.13 | 2009.03.23 | 27 | 2008.09.10 | 2009.01.20 |
| 9 | 2007.09.12 | 2008.10.03 | 28 | 2008.09.01 | 2008.12.18 |
| 10 | 2007.09.10 | 2008.05.15 | 29 | 2008.08.31 | 2010.09.15 |
| 11 | 2007.09.09 | 2009.09.03 | 32 | 2009.10.04 | 2010.01.13 |
| 12 | 2007.09.15 | 2007.12.23 | 33 | 2009.10.07 | 2011.01.24 |
| 13 | 2007.08.14 | 2008.07.16 | 34 | 2009.10.11 | 2010.11.26 |
| 15 | 2007.09.11 | 2008.10.05 | 35 | 2009.10.09 | 2010.03.30 |
| 16 | 2007.09.03 | 2008.01.01 | 37 | 2009.08.30 | 2010.12.24 |

*Note*. The missing numbers are those with few or no data due to instrument failure. The starting and ending time of ITPs are in the format of "year.month.day".

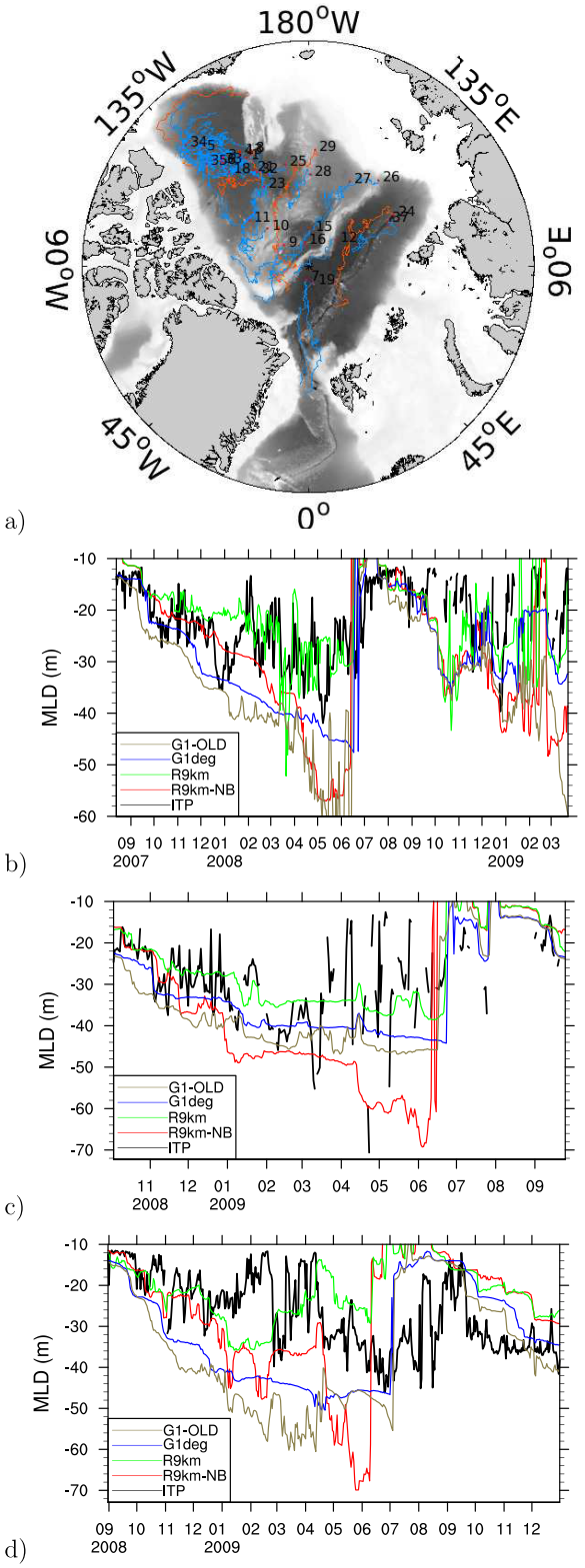


**Figure 9.** (a) ITP tracks (29 total) and comparison of modeled MLD with ITP data derived MLD along the three red tracks displayed in (b) ITP 8; (c) ITP 24; and (d) ITP 29.

future. The increasing model resolution from G1deg to R9km resulted in only a 6% reduction of MLD RMSE, much smaller than the reduction due to the brine rejection parameterization (R9km versus R9km-NB) and the sea-ice processes (G1deg versus G1deg-OLD). MLD from the three deep basins in the Arctic Ocean (red tracks in Figure 9a) are shown in Figures 9b–9d. The MLD RMSE in R9km-NB was largest from November to June, especially from March to early June. The winter MLD in G1deg-OLD was overestimated in Figures 9b and 9d, similar to R9km-NB, but matched well the observations in Figure 9c.

In a pan-Arctic view, the modeled 5 year (2005–2009) mean MLD from January to March (Figures 10b–10e) also showed similar contrasts between the four model cases. MLD from the shallowest to the deepest was R9km, G1deg, G1deg-OLD, and R9km-NB, the same order as the MLD RMSE in the comparison with ITP data. The PHC data-derived climatological mean MLD from January to March (Figure 10a) is in the middle of the four cases, but note that it is deeper than R9km because PHC data are biased toward heavier sea ice and weaker stratification in those data before 2000 compared to 2005–2009.

The January–March mean sea surface $NO_3$ (Figure 11) in the Arctic deep basin from the lowest to the higher concentrations are in the order of R9km, R9km-NB, G1deg, and G1deg-OLD, different from that of MLD in Figure 10. This suggests that vertical mixing, as defined by MLD, cannot fully explain the positive $NO_3$ bias in the Arctic Basin, and that model resolution also played a crucial, and more important role than vertical mixing in the cases we compared here. There is a large horizontal gradient of $NO_3$ from the Chukchi shelf to the Arctic Basin (see the WOA data Figure 11a), and a false horizontal diffusion due to the poorly resolved Chukchi Sea shelf break in the coarse resolution model increased the positive $NO_3$ bias in the central Arctic Basin. The horizontal mixing effect is evident from the nutrient gradients along the Chukchi Sea shelf break (Figure 11): the gradients are very strong in R9km and R9km-NB, but much weaker in G1deg and G1deg-OLD.

The modeled annual vertically integrated PP ($gC/m^2/yr$) for ice algae and phytoplankton, averaged from 2005 to 2009, are shown in Figure 12. Both ice algal and phytoplankton PP are similar for R9km and R9km-NB in most regions, except in limited areas of the Arctic Basin, where PP in R9km was lower due to lower upper ocean nutrients, as shown in Figure 10. The spatial patterns and strong gradients of PP in R9km were more aligned with bathymetric features than in G1deg, e.g., along the shelf break in the Gulf of Alaska, Bering Sea, Labrador Sea, and the northern Atlantic Ocean. PP in both ice and ocean in G1deg-OLD are lower than in G1deg in the Arctic Ocean due to stronger light attenuation through thicker sea ice in G1deg-OLD (Figure 4), although $NO_3$ in G1deg-OLD was higher. Although nutrient concentrations in the Arctic Basin of G1deg display a larger bias than in R9km, PP does not show a significant difference, suggesting that light limitation is most likely the controlling factor of phytoplankton production in this region.

A comparison of modeled sea surface $NO_3$ and Chl-a with measurements made during a 2008 Chinese arctic expedition from 12 August to 7 September (Figure 13) showed that the most significant $NO_3$ bias was in the Canada Basin from G1deg-OLD due to both coarse

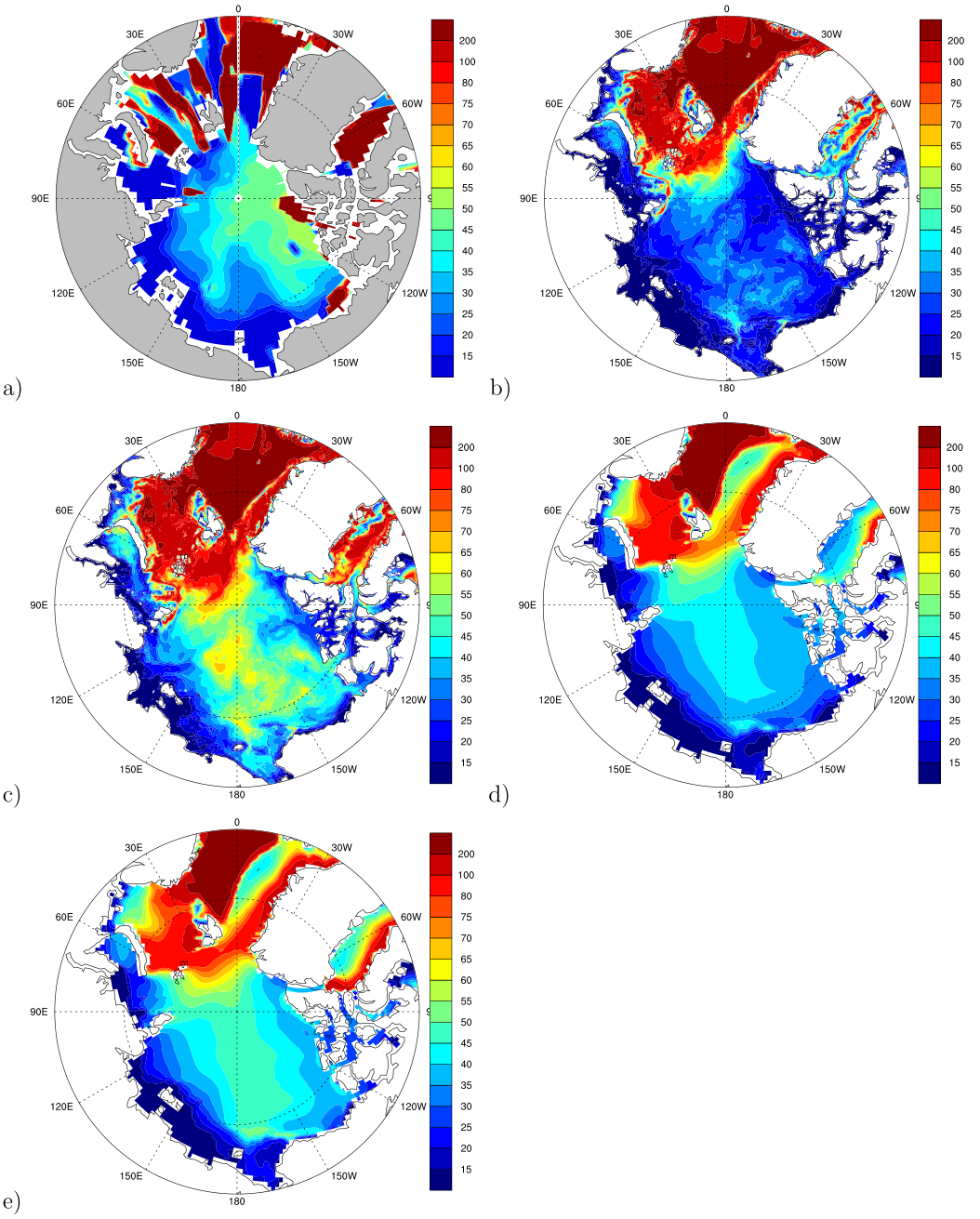


**Figure 10.** January–March averaged MLD from (a) PHC climatology data; and 5 year mean (2005–2009) of (b) R9km; (c) R9km-NB; (d) G1deg; and (e) G1deg-OLD.

resolution and deeper MLD bias, as shown in Figures 10 and 11. The $NO_3$ concentration in the Canada Basin for G1deg biased slightly higher only in some points in late August than those in R9km and R9km-NB. In contrast, there were no corresponding biases in the Chl-a concentration in the Canada Basin among all model cases, suggesting that phytoplankton growth was limited mainly by light instead of nutrients. Most of the differences in Chl-a concentration were in the first eight stations at the Chukchi and Beaufort shelf breaks, while good agreement between observations and model results occurred for the rest of the stations.

To assess where the model resolution difference between R9km and G1deg is important for BGC simulation in the Arctic Ocean, a model error comparison with in situ sea surface $NO_3$ and Chl-a data collected from 1980 to 2009 (Lee et al., 2016; Matrai et al., 2013) is shown in Figure 14, where colors denote the absolute

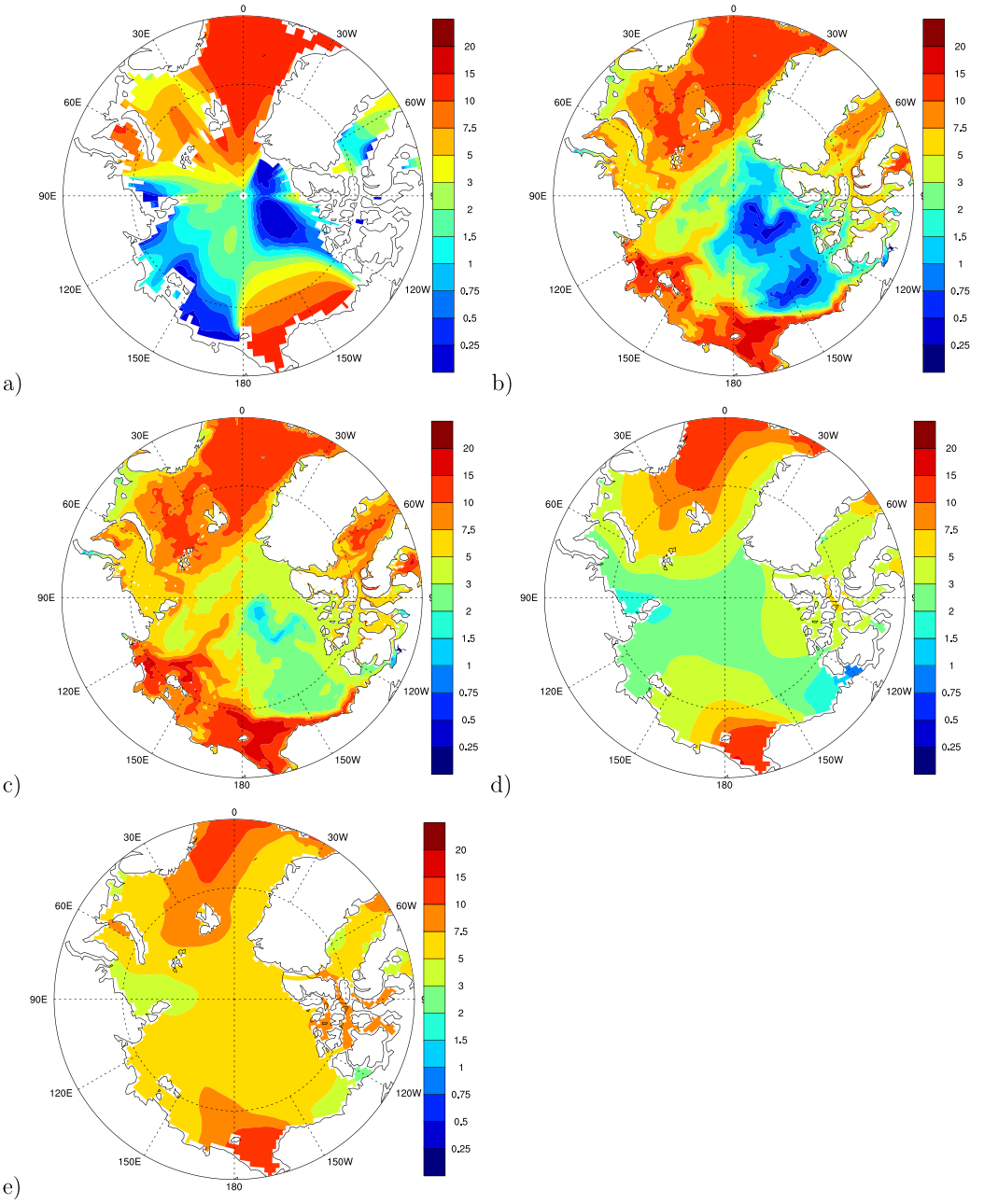


**Figure 11.** (a) January–March averaged sea surface $NO_3$ concentration from (a) WOA2013 climatology data; and 5 year mean (2005–2009) of (b) R9km; (c) R9km-NB; (d) G1deg; and (e) G1deg-OLD.

errors of G1deg minus those of R9km. The red/blue dots denote higher/lower model errors in G1deg, while black dots denote similar model errors between R9km and G1deg. Sea surface $NO_3$ concentration in R9km showed primarily lower errors in the Canada Basin and the interior of the Canada Archipelago (Figure 14a) due to the better simulated MLD (Figure 10) and less horizontal diffusion of $NO_3$ from the Chukchi Sea into the Beaufort Sea (Figure 11). For Chl-a, model errors in R9km are only lower downstream of the Bering Strait, while both cases agree in the Canada Basin (Figure 14b), suggesting that phytoplankton growth was mainly controlled by light limitation rather than nutrient limitation. Overall, the modeled nutrients showed improvements where both vertical and horizontal ocean mixing was better presented, e.g., in the Canada Basin, but Chl-a improvements might not be only linked to ocean mixing improvements as Chl-a is also strongly affected by light, especially in the Arctic Ocean.

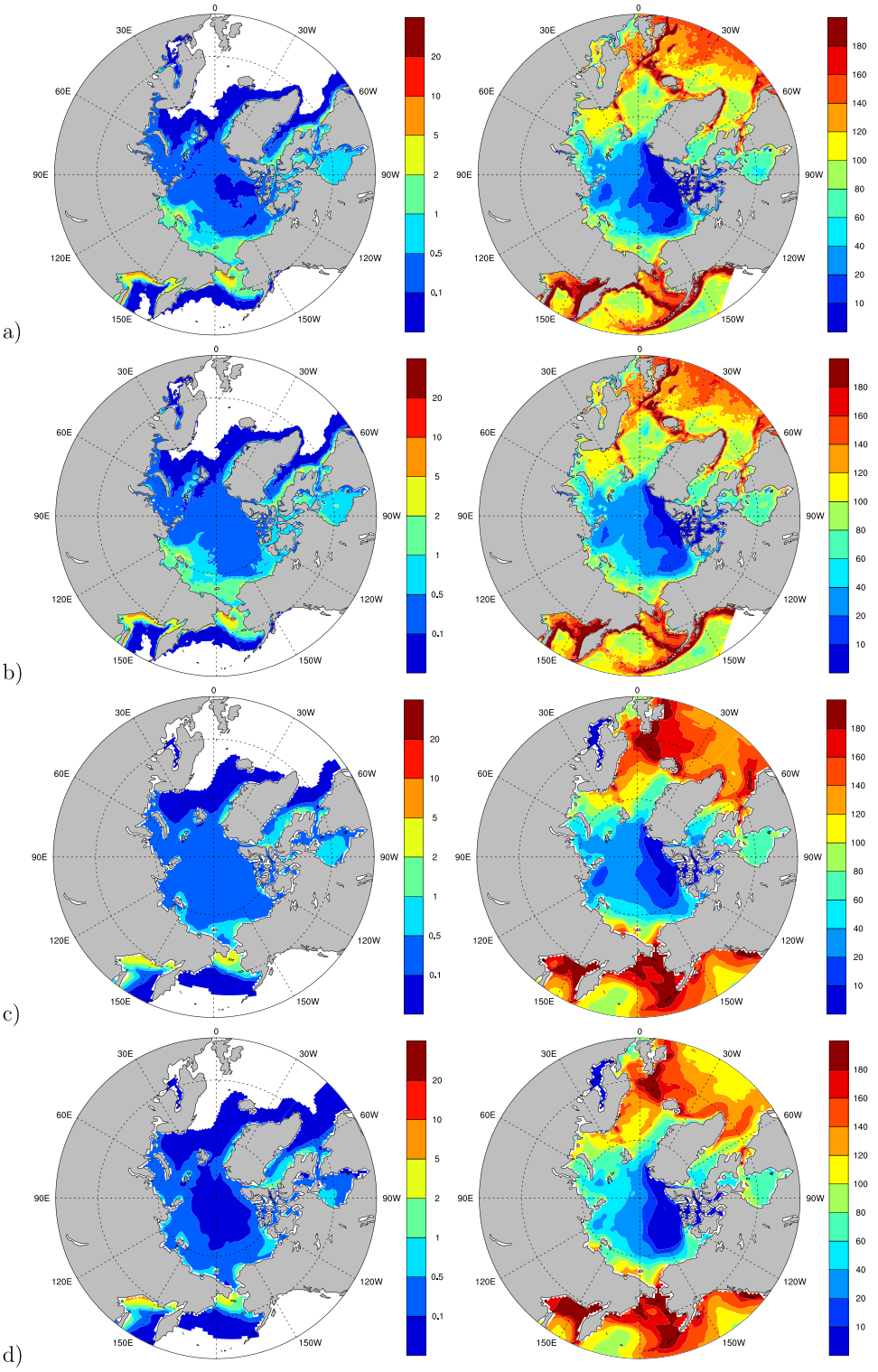


**Figure 12.** Five-year mean (2005–2009) sea-ice algae (left) and ocean phytoplankton integrated primary production (PP, mg C/m$^2$/yr) from (a) R9km; (b) R9km-NB; (c) G1deg; and (d) G1deg-OLD.

### 3.4. Subsurface Chlorophyll-a Maximum in the Canada Basin

The SCM is an important feature in the Arctic Basin which contributes significantly to vertically integrated Chl-a (Steiner et al., 2016) and is also very useful for checking a model's ability to capture the subtle balance

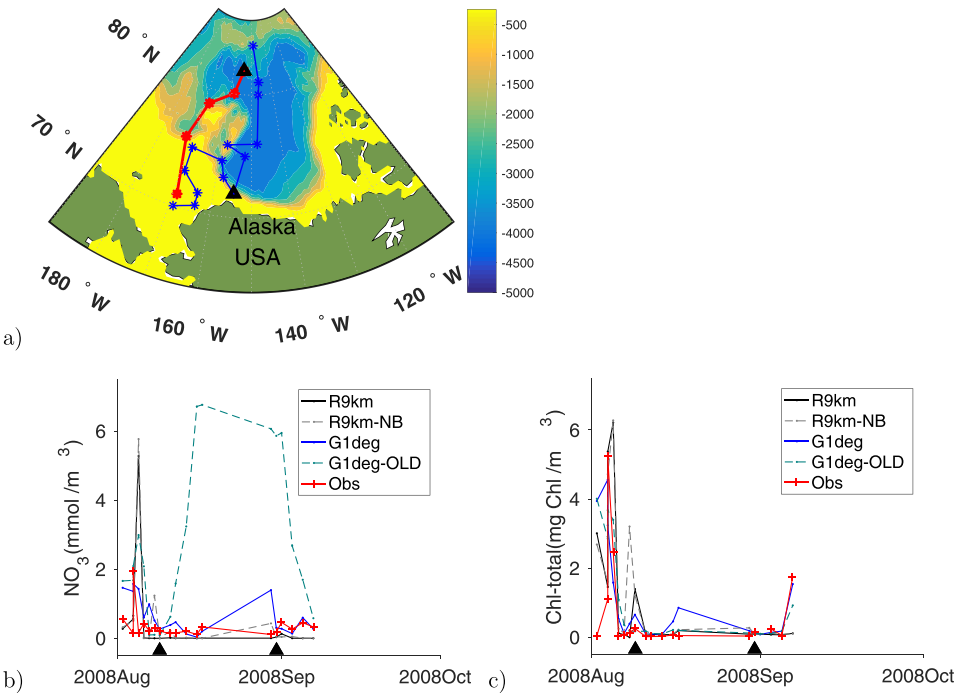


**Figure 13.** (a) Track of 2008 China Arctic cruise. The track started from the Chukchi Sea in August going northward along the blue line and back southward along the red line. Model comparison of (b) $NO_3$ and (c) Chl-a along the track. The two thick black triangles in the *x* axis of Figures 13b and 13c indicate the stations also marked in thick black triangles in Figure 13a.

between light and the deepening depth of available nutrients post phytoplankton bloom. In a previous study (Steiner et al., 2016), SCM was captured only by five out of nine ecosystem models with different resolutions and the suggested reason for failure to capture the SCM was either excessive surface nutrients or insufficient nutrients in the entire upper mixed layer. The in situ data from cruises in the Canada Basin (McLaughlin & Carmack, 2010) in August 2005 and 2006 (Figures 15a and 15b) were averaged and vertically interpolated into 10 m layers for coincident model-data comparison. Note that the observed SCM depths differed by stations and the averaged SCM depths (observed and model cases) are shown in the Figure 15. In both years, salinity, the dominant factor controlling ocean stratification in the Arctic Ocean, is similar for R9km and G1deg and closer to the observations than for the other two cases. The RMSE of salinity in R9km,

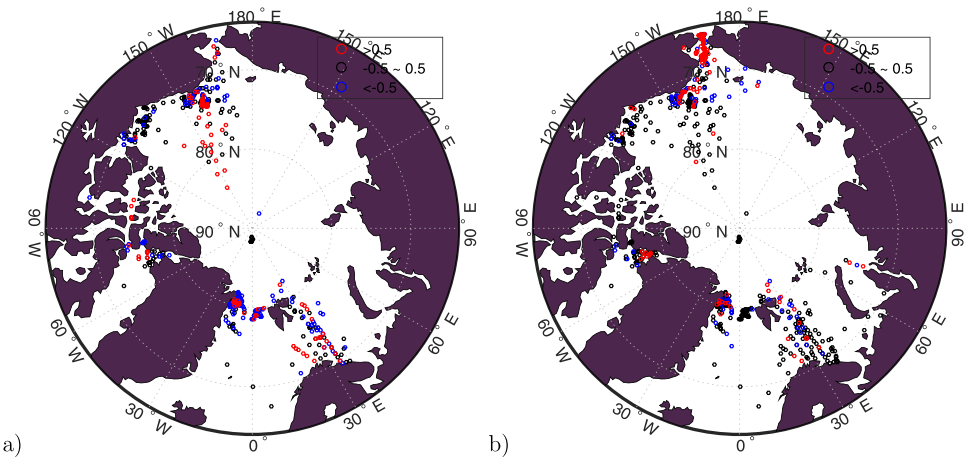


**Figure 14.** Model errors differences (G1deg minus R9km) for sea surface (a) $NO_3$ (mmol/$m^3$), (b) Chl-a (mg/$m^3$). There are a total of 500 $NO_3$ and 678 Chl-a stations. The red/blue colors denote R9km has lower/higher errors than G1deg.

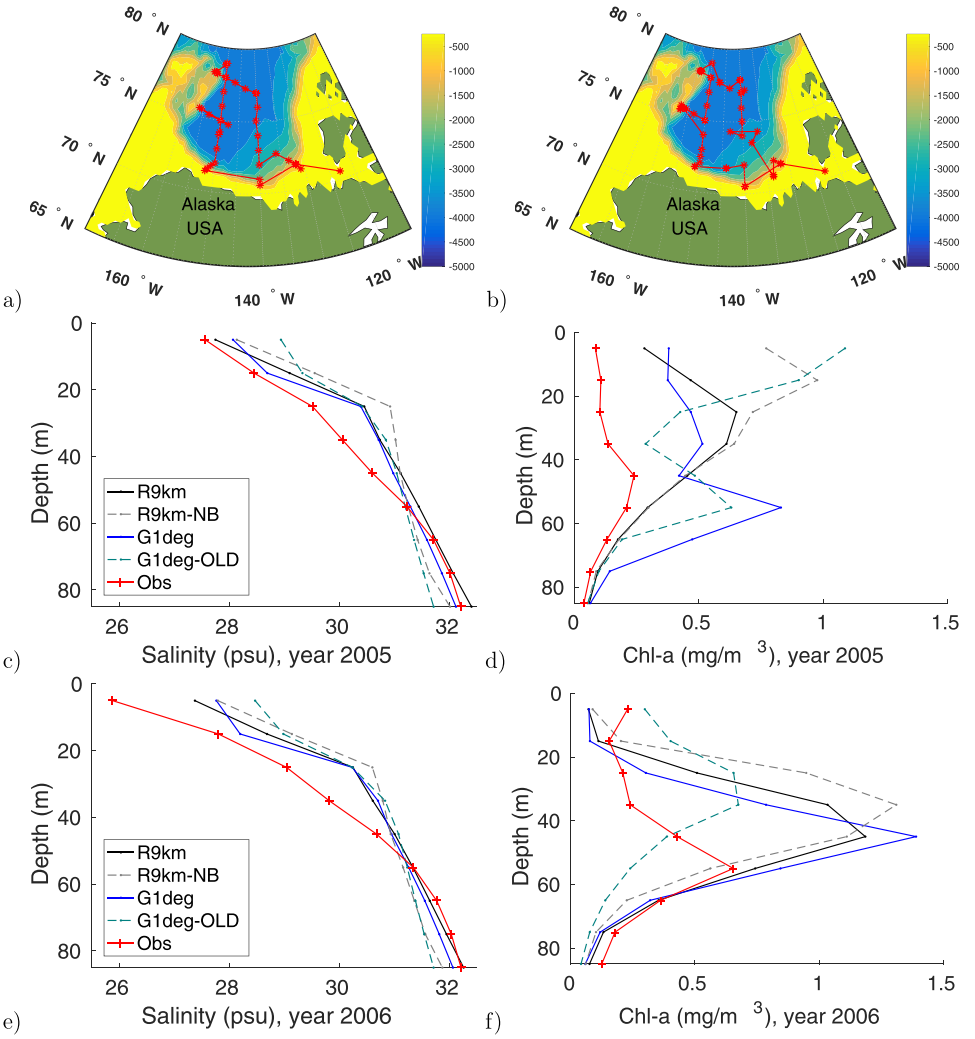


**Figure 15.** Ship measurement stations in August (a) 2005 and (b) 2006. Model comparison of averaged profiles of (c) salinity and (d) Chl-a for 2005, (e) salinity and (f) Chl-a for 2006.

R9km-NB, G1deg, and G1deg-OLD are 1.08, 1.26, 1.09, and 1.33 psu, respectively, indicating that the errors in salinity profiles are mainly caused by sea-ice processes and ocean mixing schemes rather than by model resolution. Here we do not see large errors caused by cross-shelf mixing in the coarse resolution model cases as was the case for $NO_3$, because the salinity differences between shelf and basin are much smaller than those of $NO_3$. The averaged profiles show a SCM for all cases except for G1deg-OLD in 2005, though all simulated profiles are too high in magnitude in both years. Among the total 92 profiles for the 2 years, the percentage of profiles with SCM for R9km, R9km-NB (98 and 90%) are much closer to the observations (95%) than G1deg and G1deg-OLD (79 and 52%). The RMSE of vertically averaged Chl-a in R9km, R9km-NB, G1deg, and G1deg-OLD are 0.28, 0.37, 0.35, and 0.32 mg/m$^3$, respectively. Here, for the three cases R9km-NB, G1deg, and G1deg-OLD, the lower salinity RMSE does not correspond to lower Chl-a RMSE in the Canada Basin, suggesting that the vertical profiles of Chl-a are controlled by more complicated multifactors than salinity. Overall, R9km shows less RMSE in salinity and Chl-a, and a higher skill in reproducing SCM than the other cases.

## 4. Discussion

Higher spatial resolution, and improved ocean and sea-ice processes are expected to jointly enhance model performance, as demonstrated in this study with the validations of both regional and global model

simulations. Since Popova et al. (2012) already identified the mostly positive model bias of Arctic Ocean nutrient concentrations and possible causes due to modeled MLD bias, we decided to test the following methods that improve simulated Arctic Ocean MLD: (1) a lower Arctic background mixing coefficient suggested by Zhang and Steele (2007), (2) subgrid scale brine rejection schemes applied in the Massachusetts Institute of Technology general circulation model (MITgcm) by Nguyen et al. (2009), and (3) in CESM by Jin et al. (2012a). The latter also includes the lower Arctic background mixing coefficient reported by Zhang and Steele (2007). The Jin et al. (2012b) scheme showed significant improvement in MLD after it was implemented in the high-resolution physical RASM, and was the most relevant ocean model process for the correction of MLD bias in the Arctic Ocean. Therefore, R9km-NB was selected in this study as a reference case for investigating the effects of improved ocean model processes on biogeochemistry. The five sea-ice processes and ice ocean coupling time listed in Table 2 were developed individually and each improved the physical CICE. These processes were implemented into CICE after the Popova et al. (2012) study. They collectively improved the simulation of Arctic Ocean MLD, possibly through improved ice-ocean momentum stress, heat and salt fluxes, snow depth, ice thickness and thus penetrating light reaching the ocean surface, etc. All are important factors for calculation of vertical mixing in K-Profile Parameterization (KPP, Large et al., 1997). More detailed dynamic mechanisms may deserve further studies. G1deg-OLD was also selected as a reference case in this study for investigating the collective effects of improved sea-ice model processes (Table 1) on Arctic marine and sea-ice biogeochemistry. Indeed, the comparison results confirm that the subgrid scale brine rejection scheme and the new ice processes are beneficial not only to the physical ocean and ice model results, but also to the Arctic Ocean biogeochemistry. Therefore, we suggest including these new processes in climate models.

Most of the model validation in this study is in ice covered areas, and thus significant model improvements are seen in sea surface salinity as well as MLD, but are not or less evident in sea surface temperature which is close to freezing levels with much less variability. Modeled nutrient concentrations are improved mainly due to improved vertical mixing and also partly due to improved horizontal mixing where large $NO_3$ gradients exist between the shelf and the basin, such as for the Canada Basin. Improvements in simulated nutrient concentrations do not necessarily translate into improved simulation of Chl-a or PP, especially in the Arctic Basin, where phytoplankton growth under sea-ice cover is strongly limited by light.

The observational data used for model validation in this study are limited to a few regions, mostly to the Pacific Arctic Ocean (Bering, Chukchi, Beaufort Seas, and Canada Basin), and less so to the Eurasian Basin, Fram Strait, and Barents Sea, while there are no or few data available from the Russian shelf seas (East Siberian, Laptev, and Kara Seas). The spatial distribution of the model improvements in MLD and $NO_3$ are most evident in the Canada Basin, while a less consistent spatial distribution, with mixed improved and nonimproved stations, is seen in the shallow shelf seas, e.g., Chukchi, Beaufort, and Barents Seas. Model improvements for $NO_3$ and MLD in the Eurasian Basin are not clear because there are few data available and the MLDs are deeper and more affected by North Atlantic water intrusions than those in the Canada Basin. Additional in situ data are needed from the Eurasian Basin and the Russian shelf seas for further validation of the effects on the biogeochemical responses from enhanced model spatial resolution and improved physical processes.

It is best to compare 3D biological models with time series data and large-scale spatial patterns when such data are available because biological variables, such as $NO_3$ and Chl-a, are usually highly variable in time and space. Using RMSE as a metric for model skill does not provide a means to evaluate whether the modeled large-scale spatial patterns are reasonable, but it is a useful metric to detect if most of the variables in one model case are consistently improved over other case(s) (e.g., salinity, $NO_3$ and Chl-a improvement for R9km in Table 3), especially when observations were made at different times and locations, for example, along a ship cruise track. Although fast ice is not simulated by CICE, we used observations on the fast ice for comparison in Figure 5, because this was the only time series available to us having biophysical observations at a fixed location that include a full ice algal spring bloom cycle as well as coincident snow depth and ice thickness measurements. The comparison shows that modeled snow depth, ice thickness, and nutrient environment as well as the timing and magnitude of an ice algal bloom are reasonably simulated. It is important to develop sea-ice models with fast ice (ice without motion, e.g., stuck with land or anchored to sea floor) simulation ability.

## 5. Summary and Conclusions

The RASM model has been designed to serve as a testbed for future high-resolution and high fidelity climate models in the Arctic Region. One of the key goals is to help understand and reduce model biases inherent in coarser resolution models. Sea-ice algal and pelagic ecosystem modules were incorporated into the RASM physical model framework for the first time in this study. Forced ice-ocean simulations in the pan-Arctic region show promising improvements in the higher-resolution simulations over the coarser resolution global one, which could be expected since the physical processes, e.g., mixing and transport, were improved in the higher resolution RASM configurations. It is important to note that besides increasing model resolution, improvements in the model representations of ice and ocean physical processes are also very important for improving model fidelity.

The four forced ice-ocean simulations representing different resolutions and schemes for new ice and ocean processes were validated over the Bering Sea and Arctic Ocean with various observational data, e.g., sea-ice extent and thickness, ice algae, ocean temperature, salinity, MLD, $NO_3$, and Chl-a. The sea-ice extent and thickness in R9km are improved over all other cases, especially over G1deg and G1deg-OLD, indicating higher resolution and new ice processes are important for the fidelity of sea-ice simulation. The simulated ice algal biomass in the higher-resolution regional grid cases show closer agreement with observations in the peak bloom period in the Chukchi Sea than the coarser resolution global grid cases. The modeled spatial variations of ice algal biomass in the Bering Sea matched well with observations for most of the stations for all cases, except for a few stations with larger discrepancies for the coarse resolution global grid cases. The salinity profiles for R9km compared better with observations in the Bering Sea shelf, leading to lower RMSE of $NO_3$ and MLD, which are critical for the improved simulation of ocean mixing of nutrients and Chl-a in the BGC model.

The positive MLD biases in the Arctic Ocean have been identified as the key cause for the excessively high surface nutrients (Popova et al., 2012) and a missing SCM (Steiner et al., 2016) in the Canada Basin. Here, by comparing four model cases, R9km, R9km-NB, G1deg, and G1deg-OLD, we found that the MLD biases were mainly caused by deficiencies in the ocean vertical mixing scheme shown by R9km-NB, and some model schemes representing sea-ice dynamics and thermodynamics shown by G1deg-OLD. The coarse resolution (G1deg versus R9km) contributed a relatively smaller portion to the MLD biases than the other two causes.

The modeled $NO_3$ biases in the Arctic Basin were found to be caused by both model biases in MLD and the coarse horizontal resolution grid that introduced excessive horizontal mixing of high sea surface $NO_3$ across the Chukchi Sea shelf break into the Beaufort Sea. Due to the large $NO_3$ gradients between the Chukchi Sea shelves and the Arctic Basin, the coarse resolution contributed even more to the $NO_3$ biases than the MLD biases, as seen in the comparison of MLD and $NO_3$ between R9km-NB and G1deg (Figures 10c, d and 11c, d). Improved vertical and horizontal mixing will be an asset to all biogeochemical simulations in the Arctic Ocean. Furthermore, additional in situ data from the Eurasian Basin and the Russian shelf seas will greatly benefit validation of biogeochemical simulations in those regions.

In regions with sharp bathymetric gradients (e.g., shelf break in the Gulf of Alaska, Bering Sea, and Beaufort Sea), the simulated PP distribution in the higher resolution cases retained the sharp gradient corresponding to the bathymetric features. The $NO_3$ concentrations in R9km are significantly improved over G1deg in the Canada Basin, but simulated Chl-a did not show a corresponding improvement in this region, due to light limitation persisting as the dominant factor controlling primary production under sea-ice cover in the current climate regime. Therefore, improvements of simulation of ocean stratification, light transmission parameterization, and sea-ice processes, which can affect snow depth, ice thickness, and light penetration, are all critical for better simulation of the primary production in the Arctic Ocean. Overall, higher resolution and improved schemes for the new sea-ice and ocean processes in the R9km model improved the physical model fidelity and hence the biogeochemical simulation in the Arctic Ocean, including mean states and variability.

**Acknowledgments**
This work is supported by the NSF Office of Polar Programs (PLR) 1417925 (M.J. and C.D.), 1417517 (P.M.), and 1417888 (W.M.). We thank the Regional and Global Climate Modeling (RGCM) Program of the Office of Biological and Environmental Research (BER) within the U.S. Department of Energy's Office of Science for additional support of this study. NOAA's Ecosystems and Fisheries-Oceanography Coordinated Investigations provided the fluorescence data from their long-term mooring, M2. We acknowledge NSIDC, NASA Sea-BASS, WOA, BEST, and 2008 China Arctic PIs for access to data. The supporting model outputs will be made available online (http://people.iarc.uaf.edu/~mbj/support/) after publication.

## References

Arrigo, K. R., Perovich, D. K., Pickart, R. S., Brown Z. W., van Dijken, G. L., Lowry, K. E., . . . Swift, J. H. (2012). Massive phytoplankton blooms under Arctic sea ice. *Science*, *336*(6087), 1408. https://doi.org/10.1126/science.1215065

Arrigo, K. R., & van Dijken, G. L. (2011). Secular trends in Arctic Ocean net primary production. *Journal of Geophysical Research*, *116*, C09011. https://doi.org/10.1029/2011JC007151

Bitz, C. M., & Lipscomb, W. H. (1999). An energy-conserving thermodynamic model of sea ice. *Journal of Geophysical Research*, *104*(C7), 15669–15677. https://doi.org/10.1029/1999JC900100

Boetius, A., Albrecht, S., Bakker, K., Bienhold, C., Felden, J., Fernández-Méndez, M., . . . RV Polarstern ARK27-3-Shipboard Science Party. (2013). Export of algal biomass from the melting Arctic sea ice. *Science*, *339*(6126), 1430–1432. https://doi.org/10.1126/science.1231346

Briegleb, B. P., & Light, B. (2007). *A delta-Eddington multiple scattering parameterization for solar radiation in the sea ice component of the community climate system model* (NCAR Tech. Note NCAR/TN-472+STR). Boulder, CO: National Center for Atmospheric Research. Retrieved from http://opensky.ucar.edu/islandora/object/technotes%3A484/datastream/PDF/view; https://doi.org/10.5065/D6B27S71

Cassano, J. J., DuVivier, A., Roberts, A., Hughes, M., Seefeldt, M., Brunke, M., . . . Zeng, X. (2017). Development of the Regional Arctic System Model (RASM): Near surface atmospheric climate sensitivity. *Journal of Climate*, *30*, 5729–5753. https://doi.org/10.1175/JCLI-D-15-0775.1.f

Craig, A. P., Vertenstein, M., & Jacob, R. (2012). A new flexible coupler for earth system modeling developed for CCSM4 and CESM1. *The International Journal of High Performance Computing Applications*, *26*(1), 31–42. https://doi.org/10.1177/1094342011428141

Deal, C., Jin, M., Elliott, S., Hunke, E., Maltrud, M., & Jeffery, N. (2011). Large-scale modeling of primary production and ice algal biomass within arctic sea ice resulted from the 1992 model simulation. *Journal of Geophysical Research*, *16*, C07004. https://doi.org/10.1029/2010JC006409

DuVivier, A. K., Cassano, J. J., Craig, A., Hamman, J., Maslowski, W., Nijssen, B., & Roberts, A. (2016). Winter atmospheric buoyancy forcing and oceanic response during strong wind events around Southeastern Greenland in the Regional Arctic System Model (RASM) for 1990–2010*. *Journal of Climate*, *29*(3), 975–994. https://doi.org/10.1175/jcli-d-15-0592.1

Elliott, S., Deal, C., Humphries, G., Hunke, E., Jeffery, N., Jin, M., . . . Stefels, J. (2012). Pan-Arctic simulation of coupled nutrient-sulfur cycling due to sea ice biology: Preliminary results. *Journal of Geophysical Research*, *117*, G01016. https://doi.org/10.1029/2011JG001649

Grebmeier, J. M., Oveerland, J. E., Moore, S. E., Farley, E. V., Carmack, E. C., Cooper, L. W., . . . Lyn McNutt, S. (2006). A major ecosystem shift in the Northern Bering Sea. *Science*, *311*(5766), 1461–1464.

Hamman, J., Nijssen, B., Roberts, A., Craig, A., Maslowski, W., & Osinski, R. (2017). The coastal streamflow flux in the Regional Arctic System Model. *Journal of Geophysical Research: Oceans*, *122*, 1683–1701. https://doi.org/10.1002/2016JC012323

Holland, M. M., Bailey, D. A., Briegleb, B. P., Light, B., & Hunke, E. (2012). Improved sea ice shortwave radiation physics in CCSM4: The impact of melt ponds and aerosols on Arctic sea ice. *Journal of Climate*, *25*, 1413–1430. https://doi.org/10.1175/JCLI-D-11-00078.1

Hunke, E. C. (2001). Viscous–plastic sea ice dynamics with the EVP Model: Linearization issues. *Journal of Computational Physics*, *170*(1), 18–38. https://doi.org/10.1006/jcph.2001.6710

Hunke, E. C., & Dukowicz, J. K. (1997). An elastic-viscous-plastic model for sea ice dynamics. *Journal of Physical Oceanography*, *27*(9), 1849–1867.

Hunke, E. C., Hebert, D. A., & Lecomte, O. (2013). Level-ice melt ponds in the Los Alamos sea ice model, CICE. *Ocean Modelling*, *71*, 26–42. https://doi.org/10.1016/j.ocemod.2012.11.008

Hunke, E. C., Lipscomb, W. H., Turner, A. K., Jeffery, N., & Elliot, S. (2015). *CICE: The Los Alamos Sea ice model. Documentation and user's manual version 5.1* (LA-CC-06–012). Los Alamos, NM: Los Alamos National Laboratory.

Hurrell, J. W., Holland, M. M., Gent, P. R., Ghan, S., Kay, J. E., Kushner, P. J., . . . Marshall, S. (2013). The community earth system model: A framework for collaborative research. *Bulletin of the American Meteorological Society*, *94*(9), 1339–1360. https://doi.org/10.1175/BAMS-D-12-00121.1

Jin, M., Deal, C., Lee, S. H., Elliott, S., Hunke, E., Maltrud, M., & Jeffery, N. (2012a). Investigation of Arctic sea ice and ocean primary production for the period 1992–2007 using a 3-D global ice–ocean ecosystem model. *Deep Sea Research, Part II: Topical Studies in Oceanography*, *81–84*, 28–35. doi: 10.1016/j.dsr2.2011.06.003. http://www.sciencedirect.com/science/article/pii/S0967064511001640.

Jin, M., Deal, C., Wang, J., Alexander, V., Gradinger, R., Saitoh, S., . . . Stabeno, P. (2007). Ice-associated phytoplankton blooms in the southeastern Bering Sea. *Geophysical Research Letters*, *34*, L06612. https://doi.org/10.1029/2006GL028849

Jin, M., Deal, C. J., Wang, J., Shin, K. H., Tanaka, N., Whitledge, T. E., . . . Gradinger, R. R. (2006). Controls of the landfast ice–ocean ecosystem offshore Barrow, Alaska. *Annals of Glaciology*, *44*, 63–72.

Jin, M., Hutchings, J., Kawaguchi, Y., & Kikuchi, T. (2012b). Ocean mixing with lead-dependent subgrid scale brine rejection parameterization in climate model. *Journal of Ocean University of China*, *11*(4), 473–480. https://doi.org/10.1007/s11802-012-2094-4

Jin, M., Popova, E. E., Zhang, J., Ji, R., Pendleton, D., Varpe, Ø., . . . Lee, Y. J. (2016). Ecosystem model intercomparison of under-ice and total primary production in the Arctic Ocean. *Journal of Geophysical Research: Oceans*, *121*, 934–948. https://doi.org/10.1002/2015JC011183

Krishfield, R. A., Proshutinsky, A., Tateyama, K., Williams, W. J., Carmack, E. C., McLaughlin, F. A., & Timmermans, M.-L. (2014). Deterioration of perennial sea ice in the Beaufort Gyre from 2003 to 2012 and its impact on the oceanic freshwater cycle. *Journal of Geophysical Research: Oceans*, *119*, 1271–1305. https://doi.org/10.1002/2013JC00899

Large, W. G., Danabasoglu, G., Doney, S., & McWilliams, J. (1997). Sensitivity to surface forcing and boundary layer mixing in the NCAR CSM ocean model: Annual-mean climatology. *Journal of Physical Oceanography*, *27*(11), 2418–2447.

Large, W. G., & Yeager, S. G. (2009). The global climatology of an interannually varying air-sea flux data set. *Climate Dynamics*, *33*(2–3), 341–364.

Lee, S., Jin, M., & Whitledge, T. E. (2010). Comparison of bottom sea-ice algal characteristics from coastal and offshore regions in the Arctic Ocean. *Polar Biology*, *33*, 1331–1337. https://doi.org/10.1007/s00300-010-0820-1

Lee, Y. J., Matrai, P. A., Friedrichs, M. A. M., Saba, V. S., Antoine, D., Ardyna, M., . . . Westberry, T. K. (2015). An assessment of phytoplankton primary productivity in the Arctic Ocean from satellite ocean color/in situ chlorophyll-a based models. *Journal of Geophysical Research: Oceans*, *120*, 6508–6541. https://doi.org/10.1002/2015JC011018

Lee, Y. J., Matrai, P. M., Friedrichs, M. A. M., Saba, V. S., Aumont, O., Babin, M., . . . Zhang, J. (2016). Net primary productivity estimates and environmental variables in the Arctic Ocean: An assessment of coupled physical-biogeochemical models. *Journal of Geophysical Research: Oceans*, *121*, 8635–8669. https://doi.org/10.1002/2016JC011993

Lipscomb, W. H., Hunke, E. C., Maslowski, W., & Jakacki, J. (2007). Ridging, strength, and stability in high-resolution sea ice models. *Journal of Geophysical Research: Oceans*, *112*, C3(C03S91). https;//doi.org/10.1029/2005jc003355

Li, W. K. W., McLaughlin, F. A., Lovejoy, C., & Carmack, E. C. (2009). Smallest algae thrive as the Arctic Ocean freshens. *Science*, *326*, 539–539.

Matrai, P. A., Olson, E., Suttles, S., Hill, V., Codispoti, L. A., Light, B., & Steele, M. (2013). Synthesis of primary production in the Arctic Ocean. I: Surface waters, 1954–2007. *Progress in Oceanography*, *110*, 93–106.

McLaughlin, F. A., & Carmack, E. C. (2010). Deepening of the nutricline and chlorophyll maximum in the Canada Basin interior. *Geophysical Research Letters*, *37*, L24602. https://doi.org/10.1029/2010GL045459

Moore, J. K., Doney, S. C., Kleypas, J. C., Glover, D. M., & Fung, I. Y. (2002). An intermediate complexity marine ecosystem model for the global domain. *Deep Sea Research Part II*, *49*, 403–462.

Moore, J. K., Doney, S. C., & Lindsay, K. (2004). Upper ocean ecosystem dynamics and iron cycling in a global three-dimensional model. *Global Biogeochemical Cycles*, *18*, GB4028. https://doi.org/10.1029/2004GB002220

Moore, J. K., Lindsay, K., Doney, S., Long, M. C., & Misumi, K. (2013). Marine ecosystem dynamics and biological cycling in the Community Earth System Model (CESM) [CESM1(BGC)]: Comparison of the 1990s with the 2090s under the RCP4.5 and RCP8.5 scenarios. *Journal of Climate*, *26*, 9291–9312.

Nguyen, A. T., Menemenlis, D., & Kwok, R. (2009). Improved modeling of the Arctic halocline with a subgrid-scale brine rejection parameterization. *Journal of Geophysical Research*, *114*, C11014. https://doi.org/10.1029/2008JC005121

Pabi, S., Dijken, G. V., & Arrigo, K. R. (2008). Primary production in the Arctic Ocean 1998–2006. *Journal of Geophysical Research*, *113*, C08005. https://doi.org/10.1029/2007JC004578

Peralta-Ferriz, C., & Woodgate, R. A. (2015). Seasonal and interannual variability of pan-Arctic surface mixed layer properties from 1979 to 2012 from hydrographic data, and the dominance of stratification for multiyear mixed layer depth shoaling. *Progress in Oceanography*, *134*, 19–53. https://doi.org/10.1016/j.pocean.2014.12.005

Popova, E. E., Yool, A., Coward, A. C., Dupont, F., Deal, C., Elliott, S., . . . Zhang, J. (2012). What controls primary production in the Arctic Ocean? Results from an intercomparison of five general circulation models with biogeochemistry. *Journal of Geophysical Research*, *117*, C00D12. https://doi.org/10.1029/2011JC007112

Roberts, A. F., Craig, A., Maslowski, W., Osinski, R., Duvivier, A., Hughes, M., . . . Brunke, M. (2015). Simulating transient ice-ocean Ekman transport in the Regional Arctic System Model and Community Earth System Model. *Annals of Glaciology*, *56*(69), 211–228. https://doi.org/10.3189/2015AoG69A760

Stabeno, P. J., Bond, A., Kachel, B., Salo, A., & Schumacher, J. D. (2001). On the temporal variability of the physical environment over the southeastern Bering Sea. *Fisheries Oceanography*, *10*, 81–98.

Steele, M., Morley, R., & Ermold, W. (2001). PHC: A global ocean hydrography with a high quality Arctic Ocean. *Journal of Climate*, *14*, 2079–2087.

Steiner, N. S., Sou, T., Deal, C., Jackson, J. M., Jin, M., Popova, E., . . . Yool, A. (2016). The future of the subsurface chlorophyll-a maximum in the Canada Basin - A model intercomparison. *Journal of Geophysical Research: Oceans*, *121*, 387–409. https://doi.org/10.1002/2015JC011232

Szymanski, A., & Gradinger, R. (2016). The diversity, abundance and fate of ice algae and phytoplankton in the Bering Sea. *Polar Biology*, *39*, 309–325. https://doi.org/10.1007/s00300-015-1783-z

Toole, J. M., Timmermans, M. L., Perovich, D. K., Krishfield, R. A., Proshutinsky, A., & Richter-Menge, J. A. (2010). Influences of the ocean surface mixed layer and thermohaline stratification on Arctic Sea ice in the central Canada Basin. *Journal of Geophysical Research*, *115*, C10018. https://doi.org/10.1029/2009JC005660

Tsamados, M., Feltham, D. L., & Wilchinsky, A. V. (2013). Impact of a new anisotropic rheology on simulations of Arctic sea ice. *Journal of Geophysical Research: Oceans*, *118*, 91–107. https://doi.org/10.1029/2012JC007990

Turner, A. K., & Hunke, E. C. (2015). Impacts of a mushy-layer thermodynamic approach in global sea-ice simulations using the CICE sea-ice model. *Journal of Geophysical Research: Oceans*, *120*, 1253–1275. https://doi.org/10.1002/2014JC010358

Vancoppenolle, M., Bopp, L., Madec, C., Dunne, J., Ilyina, T., Halloran, P., & Steiner, N. (2013). Future Arctic primary productivity from CMIP5 simulations: Uncertain outcome, but consistent mechanisms. *Global Biogeochemical Cycles*, *27*, 605–619. https://doi.org/10.1002/gbc.20055

Wilchinsky, A. V., & Feltham, D. L. (2004). A continuum anisotropic model of sea-ice dynamics. *Proceedings of the Royal Society of London*, *460*, 2105–2140. https://doi.org/10.1098/rspa.2004.1282

Zhang, J., Ashjian, C., Campbell, R., Spitz, Y. H., Steele, M., & Hill, V. (2015). The influence of sea ice and snow cover and nutrient availability on the formation of massive under-ice phytoplankton blooms in the Chukchi Sea. *Deep Sea Research Part II: Topical Studies in Oceanography*, *118*, 122–135. https://doi.org/10.1016/j.dsr2.2015.02.008

Zhang, J., & Steele, M. (2007). Effect of vertical mixing on the Atlantic Water layer circulation in the Arctic Ocean. *Journal of Geophysical Research*, *112*, C04S04. https://doi.org/10.1029/2006JC003732